DNA Supercoil Unwinding by Variola Virus Type IB Topoisomerase is Accelerated by

Superhelical Density and Hindered by Enzyme-DNA Interactions

by
Breeana Grogan Anderson

A dissertation submitted to Johns Hopkins University in conformity with the
requirements for the degree of Doctor of Philosophy.

Baltimore, Maryland

April 2015

Abstract

Maintenance of negative supercoils in genomic DNA is essential for diverse biological processes performed by enzymes and DNA binding proteins. Type IB topoisomerases play a key role in removing positive and negative supercoils that would otherwise accumulate at replication and transcription forks. These enzymes use a tyrosine nucleophile to cause a break in the phosphodiester DNA backbone and provide a swivel point to unwind supercoils while remaining covalently attached to the DNA via a reversible phosphotyrosine covalent linkage. An interesting mechanistic question is how topoisomerase binding, cleavage, and supercoil unwinding are regulated by the topological state of the DNA, thereby providing a mechanism for targeting the enzyme to highly supercoiled DNA domains in genomes. The variola virus type IB topoisomerase (vTopo) has unique high specificity for the target DNA sequence of 5'-CCCTT-3' and was used to execute mechanistic studies about topoisomerase function that would be challenging to perform using other type IB topoisomerases. In these studies, we have designed and synthesized supercoiled DNA minicircles (MCs) containing a single vTopo target site, providing the first highly defined substrates for exploring the effects of superhelical density on DNA binding, reversible strand cleavage, and unwinding by type IB topoisomerases. We observe that DNA binding, cleavage, and religation are independent of superhelical density. In contrast, minicircles with low superhelical densities were found to relax more slowly than highly supercoiled minicircles, suggesting that the level of torque present in the supercoiled DNA dictates how well the rotating DNA end can be captured by the enzyme to reseal the DNA backbone. This was tested with a charge reversal K271E vTopo mutant where the Lys residue is known to interact

with the rotating DNA strand. This mutant enzyme unwinds more supercoils per cleavage event, suggesting that enzyme interactions with the rotating DNA segment are important in determining the efficiency of supercoil unwinding. We infer that both superhelical density and transient contacts between vTopo and the rotating DNA determine the efficiency of supercoil unwinding. Such determinants are likely to play a role in regulating the steady-state superhelical density of DNA domains in the cell.

Thesis Advisor: Professor James T. Stivers, PhD

1st Thesis Reader: Professor James Berger, PhD

2nd Thesis Reader: Professor Roger McMacken, PhD

They have absolutely no idea what I do everyday and trying to teach science to a bunch of government contractors has been a fun challenge!

I owe my growth as a scientist and also as a critical thinker, data analyst, and troubleshooter, to Jim. When I joined his lab, I knew he was not going to make this process easy and that he was going to challenge me to be my best; he lived up that expectation. There have been frustrating times and days that I wanted switch projects, but Jim somehow always knew that this project would get done and be successful. Jim has also been incredibly open to my career goals. I was never worried about telling him that I wanted to apply my scientific knowledge to a career that had an impact on public health and policy decisions. He allowed me to work "relatively normal hours" so that I could spend the rest of my time taking classes in the School of Public Health, volunteering at the Natural History Museum, and learning about science policy and communication. I have a great respect for the mentor that he has been over the last six years and the lessons he has taught me about how to be successful in the future.

Finally, I have to thank my family. I love each and every one of them so much. My parents have been extremely supportive of my goals and have encouraged me throughout this process. My sisters cannot believe that I am still a student. And last, but most definitely not least, is my husband, Brad. Without having any idea what I mean when I complain about protein purification or an experiment not working, he keeps me positive and hopeful. Through me, he has experienced the ups and downs of getting a PhD and has provided more moral support than I could have ever imagined. I am excited to see what the future of no longer being a student holds for us!

Table of Contents

List of Tables

List of Figures

Chapter 1: Introduction

A Central Role for DNA Supercoiling

In the cell, DNA is topologically constrained in circular plasmids or anchored to the nuclear matrix, meaning that the DNA ends are no longer free to rotate as in solution[1-4]. Within these topologically constrained domains, protein:DNA interactions can introduce additional strain on the DNA, increasing its free energy and contributing to the observed steady-state negative superhelical density[5-7]. The free energy of negative DNA supercoiling serves to decrease the energy barrier for strand separation and is required to drive essential biological processes including DNA replication, RNA transcription, and DNA recombination[8,9]. Thus, maintenance of the negative steady-state superhelical density is required for proper genome function. Without this maintenance, cellular processes involving DNA would come to a grinding halt, exemplifying its biological importance [4,10-12].

DNA Secondary and Tertiary Structure

DNA is most commonly described by its helical secondary structure. This structure is energetically favorable primarily because of base-stacking and hydrogen bonding interactions. The right-handed DNA helix, in its canonical B-form, has 10.5 basepairs (bp) per twist (Tw) of the helix, with each bp rotated by approximately 36° from its adjacent pair and a rise per bp step of 3.4 angstroms[13,14]. When the B-form DNA ends are unconstrained and free to rotate in solution, the topology is described by one inherent physical property, Tw. Tw describes how the two strands of the double helix cross each other and increases with DNA length (N).

$$Tw = N / 10.5 \text{ bp}$$

In constrained DNA, the ends are held in place and an additional topological parameter, supercoiling, is introduced. Supercoiling, or writhe (Wr), is a measure of how many times the double helix overlaps with itself[7,8]. The sum of Wr and Tw is referred to as linking number (Lk) and accounts for how the two DNA strands of the double helix cross each other in a topologically constrained domain in three-dimensional space[15].

$$Lk = Wr + Tw$$

Importantly, DNA contains potential energy and is related to Lk. Lk is a constant integer value that can only change if there is a break in at least one strand of the DNA[6,15-17]. This has implications for proteins that change the Tw upon binding because local changes in Tw are partitioned into equal and opposite changes in Wr and the DNA becomes supercoiled, taking on tertiary structure[4,18]. Changes in Wr that are the result of an overwound helical state produce positive supercoils while changes in Wr that result from an underwound state are said to be negatively supercoiled[10,15](Fig 1.1).

Biological Implications of DNA Tertiary Structure

In all cells, DNA exists in an underwound, negatively supercoiled state. The quantitative level of negative supercoiling in the cell is described by the superhelical density parameter (σ), which is a quantity that is independent of DNA length[6]:

$$\sigma = Lk - Lk_o / Lk_o$$

In this equation, $Lk_o = Tw = N / 10.5$ and describes the DNA in an unconstrained environment exhibiting only secondary structure. The difference between Lk and Lk_o is a measure of the Wr, or supercoiling, that is present.

The supercoiling present in any genome represents that organism's steady-state superhelical density[1]. Generally, prokaryotic and eukaryotic DNA has a negative σ between -0.05 and -0.07, which is important for the proper initiation of many DNA transactions[19]. The strain energy present in negative supercoils destabilizes DNA secondary structure through local duplex unwinding events that allow for the formation of some protein:DNA complexes. Importantly, this includes the stimulation of critical cellular processes, such as initiation of RNA transcription and DNA replication by negative DNA supercoiling [1,6,11,15,19].

In addition to replication and transcription initiation, negative supercoiling and DNA tertiary structure are important for some DNA-binding proteins and can facilitate DNA repair[7,15]. Negatively supercoiled DNA lowers the energy barrier for duplex melting to facilitate protein:DNA interactions that depend on the protein accessing single-stranded DNA[11,19]. To promote RNA transcription, tertiary structure formed by negative supercoiling can bring distal enhancers and promoters within closer proximity, impacting gene expression and reducing search time[20-22]. Supercoiling can also enhance binding specificity between proteins and DNA in the absence of sequence specificity[23] and signal DNA damage events because of the long-range impact of DNA damage on DNA topology[10,24]. Recombination is facilitated when DNA supercoiling brings together sequences otherwise far apart in the linear DNA sequence into close proximity in three-dimensional space[1,18,23]. Importantly, the compaction of DNA that is made possible by negatively supercoiling of DNA partially explains how about two meters of human DNA containing six billion bps are compacted within a cellular nucleus that is just a few microns in diameter[10,13,15,24].

DNA Topoisomerases modify DNA Topology

Many cellular DNA transactions and protein interactions result in changes in the negative steady-state superhelical density of chromosomal DNA. These transient changes ultimately must be reversed to prevent the buildup of positive or negative DNA supercoils [1,7,8,22,25-27]. For example, during RNA transcription, melting of the DNA duplex in the transcription bubble leads to the formation of positive and negative supercoils in front of and behind the transcription machinery, respectively[28-30] (Fig 1.2). Removal of DNA supercoils can happen in at least two ways[5]. In the absence of DNA topoisomerases, the positive and negative supercoils formed during transcription diffuse along the DNA until they collide with one another, canceling each other out[28,31,32]. However, this simple scenario is rare *in vivo* for several reasons[29]. For one, if transcription occurs on two genes simultaneously in opposite directions, the supercoils will not cancel out upon collision. Second, the drag of large protein complexes on DNA unwinding hinders efficient diffusion of supercoil waves [11,20,33,34]. Thus, in the majority of cases, DNA topoisomerase enzymes are necessary[29,35-38].

Topoisomerases are the cell's solution to the topological challenges induced by excess supercoil formation [8,20,39]. One, and often two or more, functional topoisomerases are required in many organisms to relieve topological strain[9]. All topoisomerases act by using an active site tyrosine residue to perform nucleophilic attack on the DNA phosphodiester bond, cleaving it and creating a covalent phosphotyrosine linkage and nick in the DNA backbone[40]. This nick allows changes in Lk because the DNA is no longer constrained and the Wr component can be fully or partially removed[36]. The enzyme releases and turns over because the favorable leaving group property of the

4

phenolic hydroxyl makes the cleavage reaction reversible. The DNA backbone is reformed via nucleophilic attack of the free sugar hydroxyl group at the phosphotyrosine linkage; this reverse process is known as strand ligation[35].

Topoisomerases are a diverse class of enzymes that can be split broadly into the type I and type II families[36,38,40,41]. Most higher order organisms contain at least one type I and one type II topoisomerase[9]. Type I topoisomerases are monomers that form a single-stranded nick in the DNA without needing an energy cofactor[35]. In contrast, type II topoisomerases are dimers that form a staggered double-stranded break and use ATP hydrolysis as energy to drive conformational changes that lead to supercoil unwinding[42]. The type I topoisomerase family is further split into type IA (the identity of the first topoisomerase discovered in *E.coli*) and type IB (found primarily in eukaryotes). The two subfamilies do not arise from a common ancestor and are mechanistically distinct[43]. The type IB subfamily (topoIB), which is the focus of this work, shows structural similarity with the tyrosine recombinase superfamily of enzymes that also use a phosphotyrosine intermediate to facilitate DNA strand exchange and recombination[9,44,45].

Topoisomerase DNA Unwinding Mechanism

Each family of topoisomerases has developed a unique mechanism for efficiently maintaining negative superhelical density. The type II topoisomerase family adds or removes two supercoils per cleavage event, changing DNA linking number in increments of two[35,36,40,46,47]. The type IA topoisomerase subfamily recognizes single-stranded regions of the genome caused by excess negative superhelical density and uses Mg^{2+} to remove negative supercoils in a stepwise fashion (termed "strand passage"), with each cleavage event followed by the release of a single supercoil prior to strand ligation[35,48,49].

This subfamily includes the type I enzymes found in bacteria and archaea and the type III enzymes found in eukaryotes[44]. The type IB topoisomerases act on double-stranded DNA to relax both positive and negative supercoils in increments of one linking number [50,51]. In contrast to the "strand passage" supercoil release mechanism used by type II and IA topoisomerases, topoIB uses a stochastic "controlled rotation" mechanism where more than one supercoil can be removed for each cleavage event [9,52-54].

The controlled rotation mechanism of topoIB is partially explained by its structure when bound covalently to DNA. The enzyme clamps circumferentially (Fig. 1.3A) around the DNA duplex, forming a 3' phosphotyrosine linkage and expelling a free 5'OH immediately following the nick. The DNA downstream of the nick is free to rotate around the DNA axis of the intact strand, efficiently unwinding supercoils[42,43,55-57] (Fig. 1.4). Torsional strain built up in supercoils from DNA replication or transcription can be rapidly released so that these same processes proceed unimpeded. The number of supercoils unwound per cleavage event is dependent on the average rate of supercoil unwinding (k_{uw}) and the lifetime of the covalent complex[53]. The lifetime of the covalent complex is given by the time constant for strand ligation (k_{lig}). For both linear and circular, supercoiled substrates, the DNA strand cleavage equilibrium, K_{cl} ($K_{cl} = k_{cl}/ k_{lig}$) is around 0.1, indicating that the intact DNA state is favored approximately ten times more than the cleaved state and that k_{lig} is faster than k_{cl}[53]. The unwinding rate is dependent on the rotational torque present in the positive or negative DNA supercoils[54]. Although topoIB catalyzes supercoil release by nicking the DNA backbone, it actually controls the unwinding rate through interactions with the rotating downstream DNA and positively charged residues that create frictional resistance to duplex rotation [4,54,58,59] (Fig.

1.3B). Controlled rotation is likely important for facilitating enzyme capture of the mobile DNA segment and the subsequent positioning of the 5'-OH DNA relative to the phosphotyrosine linkage that is essential for strand ligation[44].

The controlled rotation mechanism for supercoil removal has relevance to pharmacological aspects of topoIB action. In the presence of the chemotherapeutic drug irinotecan or topotecan (members of the camptothecin class of small molecules that bind to the topoIB covalent complex[60,61]), strand ligation in human topoIB is hindered because the bound drug sterically blocks the 5'-OH from approaching the covalent phosphotyrosine linkage[62]. In this case, the cleavage equilibrium (K_{cl}), the lifetime of the covalent complex, and the concentration of the covalent complex will increase [44,63,64]. If k_{uw} remained unchanged by drug binding, all DNA supercoils would unwind before ligation had a chance to seal the strand break. . In contrast, if k_{uw} was greatly diminished by drug binding, fewer supercoils would be removed prior to a strand ligation event and supercoils would accumulate in the cell during DNA replication and RNA transcription. Experiments show that the actions of these drugs increase the lifetime of the covalent complex and decrease the unwinding rate of positively supercoiled DNA[63]. Accumulation of positive supercoils in actively replicating cells ahead of the replication machinery can lead to replication stalling, fork collapse, and double-stranded breaks. In cancer cells undergoing increased cell division, this topological imbalance, in the absence of efficient repair, often leads to cell death[63,65].

Thesis Question and Hypothesis

Extensive experimental work has been performed to understand the topoIB mechanism. Biochemical and structural research have provided insight into each discrete

mechanistic step – DNA binding, cleavage, supercoil unwinding, strand ligation, and enzyme release. Combined structural and mutagenesis studies have elucidated important residues and conformational states required for enzyme activity[44,50,51,56,59,66,67]. Despite this wealth of information, an important and poorly understood aspect of the topoIB mechanism is how DNA tertiary structure, or the degree of DNA supercoiling, affects each step[7]. Efficient topoIB activity relies on the enzyme being able to actively sense and respond to discrete changes in steady-state superhelical density. The work in this thesis aims to determine how the specific steps in the topoIB mechanism are influenced by superhelical structure of the DNA.

Upon initiation of these studies, we hypothesized how DNA supercoiling might specifically facilitate targeting of topoIB to supercoiled regions or enhance the subsequent steps of the reaction. First, it was possible that topoIB could be specifically targeted to regions with increased superhelical density due to a greater binding affinity of the enzyme for this type of DNA structure as compared to relaxed or linear pieces of DNA[38]. Second, we considered that changes in superhelical density could impact the rate of phosphodiester bond cleavage by topoIB. In this case, DNA nodes or the degree of DNA curvature could impact transition state binding interactions that would lower the activation barrier of the reaction[53,68-70]. Third, DNA unwinding rates may be greater for highly supercoiled DNA due to larger torsional strain in the DNA that might drive the unwinding rate[4,8,53,54]. If during rapid unwinding, the efficiency of strand capture were decreased, a greater number of supercoils would be unwound per cleavage event. The unwinding rate would then slow as the superhelical density decreased and at a certain

8

level, there might be multiple cleavage and ligation cycles before another supercoil was removed [53,71].

Recognition of Supercoiling during DNA Binding

As mentioned above, one potential mechanism by which topoIB could target and act at regions of increased superhelical density is by preferentially binding supercoiled DNA[44,68,72]. This type of mechanism is attractive because the difference between substrate and product in the topoIB reaction is not chemical, but structural in nature. TopoIB recognizes and relaxes both positively and negatively supercoiled DNA[35]. Therefore, we expected recognition to take place via a structural feature that was common to both superhelical forms. Possible features of supercoiled DNA that could drive recognition include superhelical nodes (places where the DNA duplex crosses itself) or increased curvature arising from torsional strain [73,74]

This question of whether supercoiling affects enzyme binding has been explored previously using filter binding and EMSA assays[75]. In these binding studies, it is advantageous to use an inactive Tyr to Phe topoIB mutant to prevent DNA relaxation[75,76]. Alternatively, kinetic competition experiments can be performed using the wild type enzyme[72,77,78]. In both types of assays, topoIB appears to bind substrates with increased topological strain or superhelical density better than relaxed circular DNA. The EMSA assays have limitations because they use high protein to DNA ratios that can give rise to protein oligomerization on the DNA (see below) [76,79]. A recent study using a filter binding assay that minimized protein oligomerization and inactive topoIB reported a much weaker preference of human topoIB for supercoiled DNA[80].

9

Another method for addressing whether topoIB preferentially binds superhelical DNA is through the use of electron and atomic force microscopy. Although microscopy imaging studies are useful to visualize the topo:DNA complex, large ratios of protein to DNA are used in these methods which can lead to oligomeric structures that may not be biologically relevant. For instance, in an AFM study of vTopo binding to pGEM plasmid DNA, filaments of vTopo were observed to assemble on the DNA as the protein to DNA molar ratio was increased from 3:1 to 60:1. The authors suggested that vTopo binding to form filaments on DNA is thus cooperative in nature[81]. These experiments make it hard to determine whether increased binding of topoIB to supercoiled DNA is a biologically relevant recognition mechanism. Other studies suggest topoIB preferentially binds at nodes where the DNA duplex crosses itself [7,38,73,77,81-83]. One possibility is that vTopo dimerizes upon binding DNA and these nodes are the result of two enzymes coming together and synapsing the DNA strands with them[82]. Alternatively, it is possible that the enzyme does not actually bind preferentially to preexisting nodes, but instead creates new nodes upon binding. In this case, topoIB is actually introducing torsional strain into the DNA. In this type of process, topoIB would first bind to a single piece of DNA duplex and then use a second DNA binding site to bring in another duplex region[79]. Since this mechanism requires two DNA binding sites, a large amount of work has focused on confirming whether two duplex binding sites are present on topoIB when crystal structures show only one DNA binding site[57,67]. EMSA and filter binding experiments have shown that human topoIB has a conserved region distant from the primary DNA binding site that can interact with DNA to induce superhelical nodes[79]. In support of the secondary binding site hypothesis, recent crystal structures of a bacterial topoIB reveal

10

the presence of a group of conserved positively charged residues on the C-terminal domain. Mutagenesis experiments that remove these residues resulted in a decreased propensity of the enzyme for forming superhelical nodes and introducing torsional strain[84,85].

vTopo Mechanistic Studies

Topoisomerase IB from poxvirus (vTopo) has served as a useful model system to study DNA binding, strand cleavage and ligation, and DNA unwinding. The cleavage and ligation steps have been studied in detail using short linear DNA oligos containing a single specific cleavage site[86-89], but information about supercoil unwinding has been limited to the use of large supercoiled plasmids[53]. In the late 1990s, circular pUC19 plasmid DNA with 17 vTopo recognition sites was used to provide an in depth study of the vTopo supercoil unwinding reaction[53]. Specifically, a new kinetic framework for analyzing supercoil relaxation was introduced and used to determine that supercoil unwinding followed a stochastic "free rotation" mechanism where more than one supercoil was removed per cleavage and ligation cycle[53]. One limitation to this early approach was that multiple CCCTT sites existing on a single plasmid make it difficult to be sure that a single topoIB was acting per plasmid, although conditions were adjusted to favor this condition. Despite this caveat, the study indicated that strand cleavage and ligation and enzyme dissociation were not greatly affected by DNA topology[53]. In addition, the study showed that an average of five supercoils are removed per cleavage event with a supercoil release rate of at least 20 s^{-1} [53]. Unlike a nicking enzyme that would cause rapid and complete removal of all supercoils following strand break without the possibility for ligation, vTopo ligation traps quantifiable amounts of partially relaxed,

intermediate populations of topoisomers[53]. Due to additional limitations arising from a large plasmid with many cleavage sites and fluorescence imaging technology at the time, this study could not make definite conclusions regarding the topological dependence of supercoil unwinding. A later study in 2012 returned to this vTopo-pUC19 system using enhanced imaging and analytical methods[58]. This study used vTopo mutants to show that positively charged protein residues interacting with the negatively charged, rotating DNA backbone were responsible for limiting the number of supercoils unwound per cleavage event[59] (Fig. 1.5). It was concluded that the mutants increase the lifetime of the covalent complex by decreasing ligation rates, increasing the unwinding rate of the enzyme, or both[58].

TopoIB Single Molecule Studies

The single molecule field saw topoisomerases and supercoil unwinding as an interesting system for investigation[4,8,35]. Researchers developed methods to constrain DNA by anchoring it to an immobile surface on one end and then to a paramagnetic bead on the other end. Small magnets placed above the paramagnetic bead could then control the stretching force applied to the system and the degree of supercoiling. As supercoiling increases at constant force, torque, or the rotational potential energy in the DNA, increases[15]. As supercoiling continues to increase, a critical point is reached so that torque becomes constant and all additional energy added to the system is partitioned to writhe, as evidenced by a change in the position of the magnetic bead and decrease in the DNA extension length[54]. Thus, at constant applied force, the process of topoisomerase-mediated DNA unwinding can be followed[8].

Single molecule experiments have now been used to study the mechanisms of many classes of topoisomerases and qualitatively confirm earlier observations that topoIB DNA unwinding follows a free rotation mechanism[4]. In a single molecule experiment with vTopo, the presence of a constrained segment of lambda phage DNA containing 63 topo recognition sites also provided further insight into the DNA unwinding reaction[54]. By varying the force applied to positively supercoiled DNA and then observing changes in DNA extension following the addition of vTopo, the release of supercoils could be followed in real-time. Under these conditions, unwinding events are sensitive to the force applied to the DNA and the number of supercoils unwound per cleavage event increased with increasing applied force. On average, about 19 supercoils were released per cleavage event. The vTopo unwinding rate was experimentally compared to that of nicking enzymes that cannot ligate DNA and hTopo (human topoIB), which buries a larger DNA surface area downstream of the nicking site[67]. The unwinding rate for nicking enzymes was faster than vTopo while the rate for hTopo was slower[54]. This difference in unwinding rates with different topoIBs suggests that interactions with the mobile DNA segment can be described by an effective frictional coefficient for duplex rotation[44]. These single molecule experiments led researchers to propose a model whereby the energy landscape of topoisomerization is tilted and driven by the torque present in the DNA. While the authors expect similar results with negatively supercoiled DNA, the constraints of the system through application of external force prevented confirmation of this hypothesis[54].

Single molecule experiments have also shed light on the competition between strand ligation and supercoil unwinding. It is unclear exactly what structural event causes

ligation to interrupt the supercoil unwinding process but the overall process of strand ligation is competitive with supercoil unwinding rates because partially supercoiled intermediates are observed during supercoil unwinding of a highly supercoiled plasmid [58,75,90]. Recent modeling work and additional single molecule studies have suggested that ligation occurs during a stochastic pausing event in supercoil unwinding[44]. Along the supercoil unwinding free energy pathway, there are periodic maxima that modulate the rate of supercoil unwinding while minima provide a metastable ligation competent conformational state[71]. There may be a conformational change that takes place from an open state competent for DNA unwinding to a closed state where the DNA can ligate [64,71].

This conformational change suggests that the probability of topoIB for ligation would depend on how long and how often the DNA enters this closed state, which may also be force dependent in single molecule experiments. Single molecule studies suggest that increasing force can impact the number of supercoils unwound per cleavage event by decreasing the probability for strand ligation but there are limitations in the interpretation of this finding [54,64]. The measurements do not make it clear whether the decreased probability of ligation is due to a decrease in the ligation rate at high forces or an increase in the unwinding rate that would allow more supercoils to be unwound before ligation takes place. As with previous ensemble experiments, an important limitation of these experiments is the large number of topoIB recognition sites present on the DNA substrate. It is unlikely that all of the sites share the same kinetic properties because cleavage and ligation are known to be sensitive to sequence differences even for specific vTopo sites[51].

Variola Virus Topoisomerase IB

TopoIBs have commonly been studied in humans (hTopo) and members of the poxvirus family (vTopo). hTopo with 765 amino acids is more than twice the size of the vTopo with 314 amino acids but the two share sequence and mechanistic similarities, making vTopo an excellent prototype for the topoIB subfamily[56,62,80,81,91]. In addition to its small size, vTopo preferentially recognizes, binds, and reacts at a specific pentapyrimidine sequence containing 5'-(C/T)CCTT-3' [51]. This sequence specificity makes kinetic and thermodynamic study of vTopo, historically on short oligos containing a single recognition sequence per substrate, possible[87]. hTopo does not exhibit such sequence specificity and reacts at a multitude of sequences with a weak preference for (A/T)(G/C)(A/T)T[35]. Using the crystal structure to guide mutational analysis, a previous study in the Stivers lab showed that mutation at Lys271 (and several other cationic residues that interact downstream of the nick created by phosphotyrosine covalent complex formation) increases the number of supercoils released per cleavage event[58,59]. The studies presented here have all been performed using wild type and mutant variola virus topoIB, the topoisomerase used by the smallpox virus, as the prototypical topoIB[92].

Physiologically, vTopo is essential for efficient replication and transcription during the viral life cycle[93]. It is a double-stranded, linear DNA virus and replicates entirely in the cytoplasm of infected cells, thus the need to encode its own topoisomerase[67,82,92]. Deletion of topoisomerase has been shown to selectively impair transcription by a virally encoded RNA polymerase during the early phases of the viral life cycle, suggesting a role for vTopo in viral infectivity[79,92,94].

Engineered DNA Minicircles Substrates

All previous experiments with vTopo in the literature have used either short duplex oligonucleotides containing a single CCCTT vTopo recognition site [86,87], or supercoiled plasmids containing multiple CCCTT recognition sites that can complicate kinetic analyses for these substrates [53,54]. The presence of multiple vTopo recognition sites also makes it difficult to study the effect of supercoiling on binding in the absence of sequence effects. Because of these limitations, we set out to design topologically constrained circular substrates with customizable sequences, sizes, and superhelical densities. To do this, we used recent technology developed to create DNA minicircles for gene therapy applications[53,95,96]. This provides us the ability to amplify large amounts of plasmid DNA containing the proper replication promoter sequences and antibiotic resistance before using *in vivo* recombination in bacteria to separate the dispensable portion of the expression plasmid from the portion of the plasmid containing the minicircle sequence of interest, which can be constructed using gene synthesis methods[53,58,59,97-101].

Our completely customizable minicircle sequence, containing either a single CCCTT site or devoid of any related pentapyrimidine sequences, has several features that facilitate mechanistic studies on vTopo. First, since only one or no cleavage sequences are present in the minicircles, the reaction kinetics are simplified and the background rate of supercoil relaxation arising from DNA cleavage at non-specific sites can be quantified for the first time. Second, the size of the minicircle can be changed to test the effect of size on the kinetics of site-specific recognition. By using smaller minicircles, we have the advantage of being able to cleanly separate individual topoisomers using agarose or

acrylamide gel electrophoresis and quantify the appearance and/or disappearance of product, substrate, and intermediate. Third, we can manipulate the superhelical density of our minicircles without the need to apply an artificial external force during the topoIB reaction by using ethidium bromide (EtBr) supercoiling techniques[58,102-104](Fig. 1.6).

Using our unique minicircle DNA substrate and vTopo, we show that DNA binding is independent of superhelical density but sensitive to changes in DNA length. We are also able to apply a simple model to our supercoil unwinding experiments to show that cleavage and ligation are not sensitive to DNA topology but highly supercoiled substrates release more supercoils per cleavage ligation event than substrates with decreased numbers of supercoils. In the case of low superhelical density intermediates, the enzyme may actually undergo multiple cleavage and ligation events prior to the release of a further supercoil. The control that vTopo exerts on the unwinding rate is dependent in part on Lys271 and by inference, other enzyme interactions with the downstream DNA. Mutation of Lys271 increases the number of supercoils unwound per cleavage event and decreases the control that vTopo exerts on the rate of supercoil unwinding.

Figure 1.1 $N = 105$ bp $Lk_o = Tw = 105/10.5 = 10$ $\Delta Lk = Lk - Lk_o = 0$

Tw Decreases $\Delta Lk = Lk - Lk_o = -2$

$N = 105$ bp $Lk = Tw + Wr$ $8 = 10 + -2$
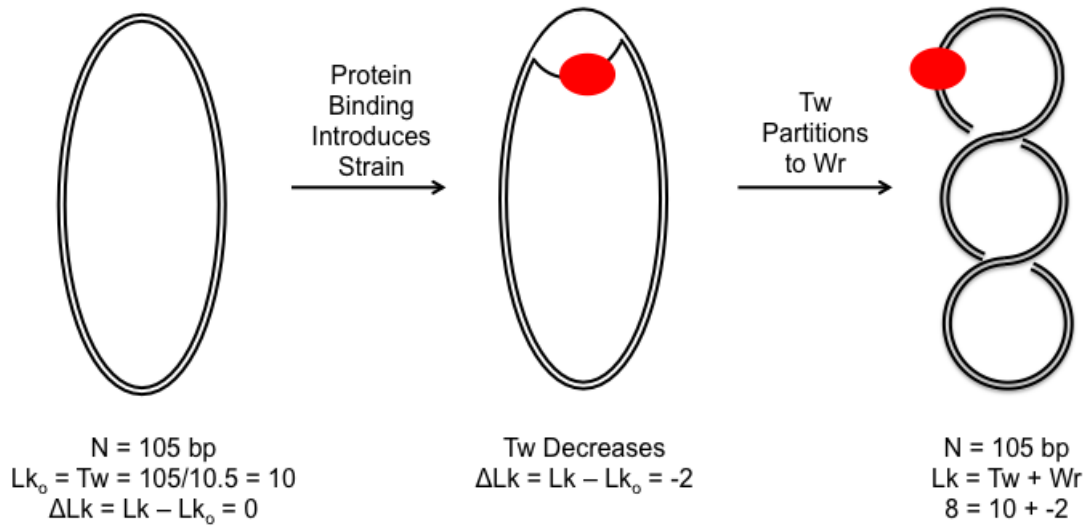
Figure 1.1 Constrained Topological Domains have Twist and Writhe.
A piece of DNA N bps in length can be described by its Lk. Lk is the sum of Tw and Wr. In the absence of strain, DNA is described only by its Tw, which is a function of N and has 10.5 bps per turn. In the presence of strain, Lk must remain constant, so changes in Tw are partitioned to changes in Wr as Tw returns to its native 10.5 bps per turn. A negative change in Wr is accounted for by the formation of negative, right-handed supercoils.
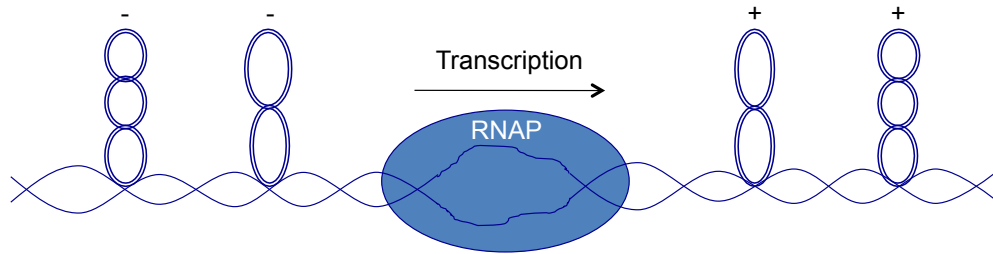
Figure 1.2 Cellular Processes induce changes in Steady-State Superhelical Density.
Transcription is just one example of a cellular process that acts to distort DNA superhelical density. As the transcription machinery moves along the double helix, a transcription bubble forms, changing the Tw of the DNA as it undergoes transcription. This change in Tw is accounted for by the formation of positive supercoils in front of the fork and negative supercoils behind the fork. The supercoils must be removed by diffusional collision of canceling superhelical waves or different sign or the actions of topoisomerases.
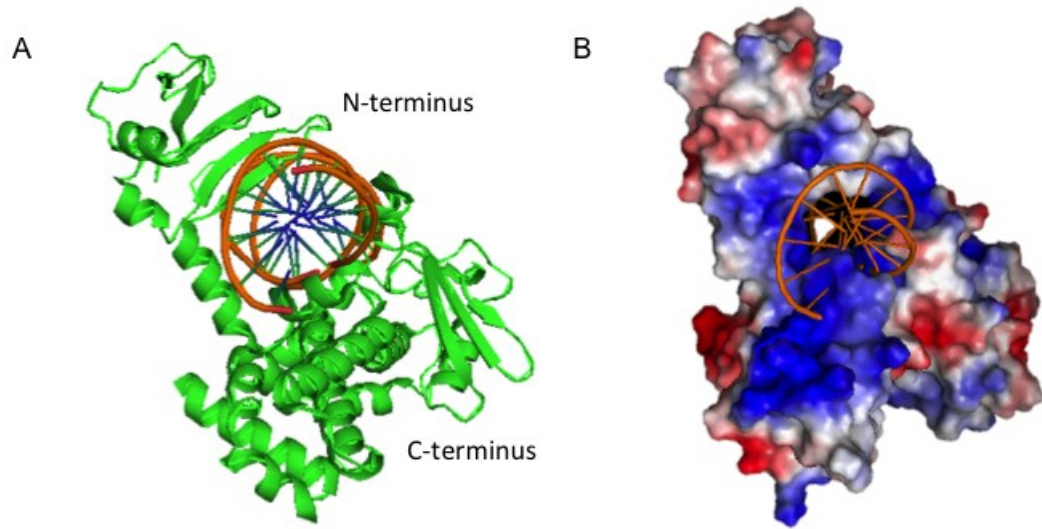
Figure 1.3 Crystal Structure of the Variola Poxvirus Topoisomerase IB in complex with DNA.

(A) TopoIB binds DNA circumferentially, forming a clamp-like structure around the duplex. The conserved active site tyrosine is contained within the C-terminus. (B) Blue represents positively charged protein residues while red corresponds with negatively charged residues. The large positively charged protein core shown in this space-filling model allows the protein to interact electrostatically with the DNA backbone.
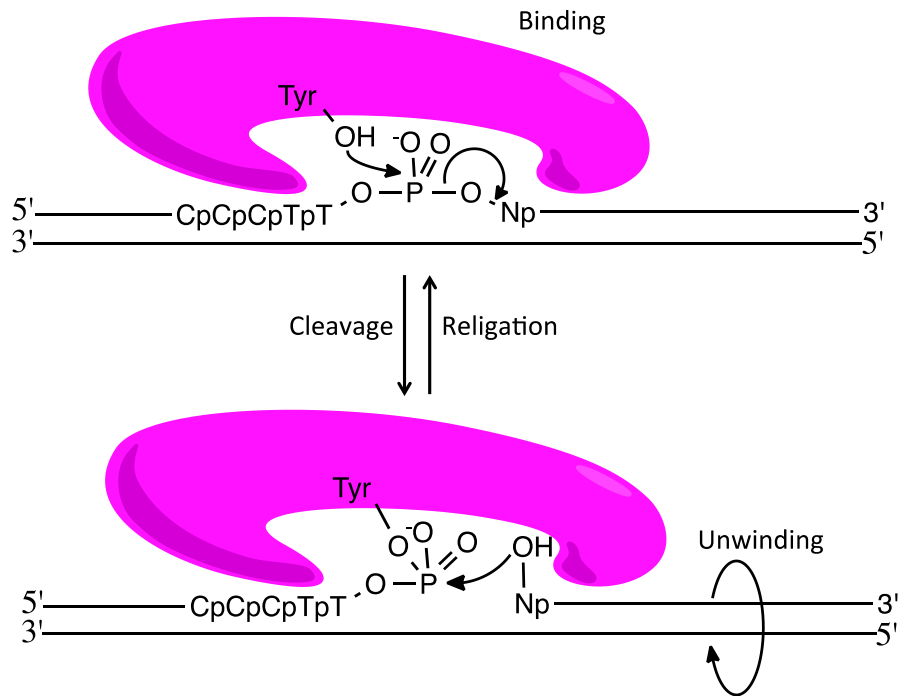
Figure 1.4 Topoisomerase IB Supercoil Unwinding Mechanism.
Upon binding DNA, topoIB uses a conserved active site tyrosine to create a phosphotyrosine covalent complex via nucleophilic attack. The lifetime of this covalent complex determines the number of supercoils unwound per cleavage event. Supercoil unwinding involves rotation of cleaved strand around the helical axis and can only occur during the lifetime of the covalent complex. The unwinding process stops once DNA strand ligation occurs.
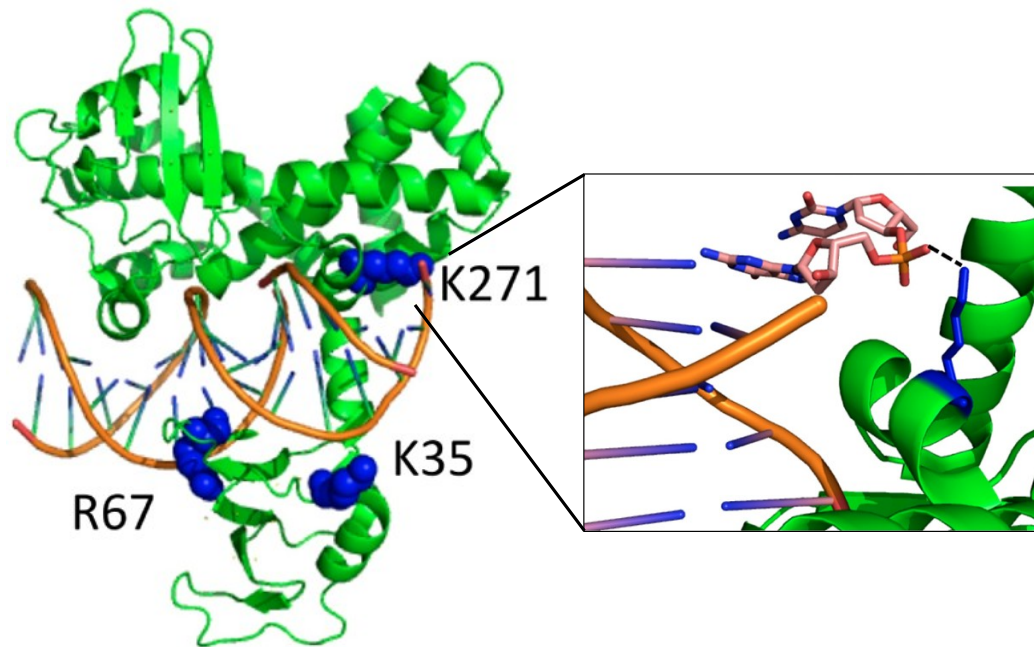
Figure 1.5 Positively-charged Protein Residues make Important Interactions with Downstream Mobile Segment of Cleaved DNA.
Upon mutation of K271, K35, and R67 to Ala or Glu, an increased number of supercoils were removed per cleavage event[8,15,54,58,59]. These residues, especially K271, are important in dictating the efficiency of supercoil unwinding.
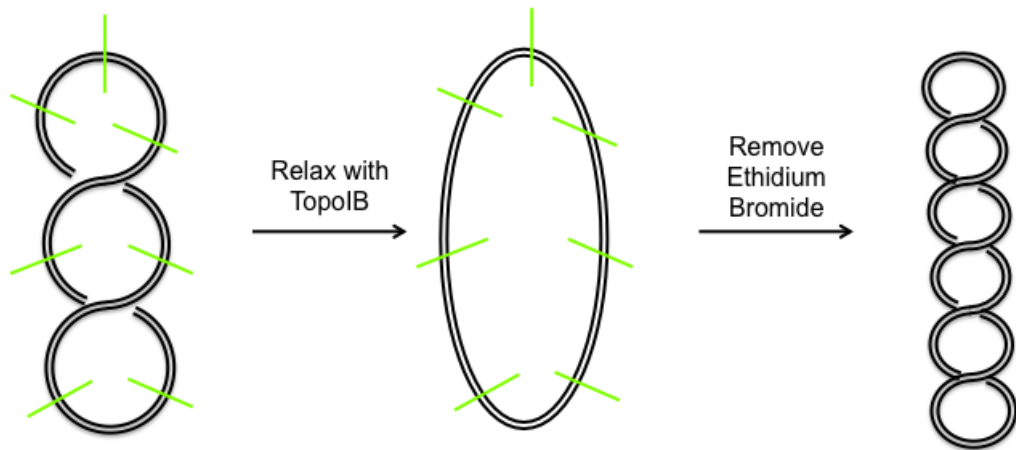
Figure 1.6 Ethidium Bromide-mediated Supercoiling.
The intercalation of ethidium bromide into DNA increases the number of bps per turn of the double helix. When supercoils are relaxed by topoisomerase in the presence of ethidium bromide, this increase in twist is captured as the enzyme seals the strand break. Upon the removal of ethidium bromide and the topoisomerase, the DNA relaxes back to its natural Tw of 10.5 bp/turn. Because the backbone is sealed, the excess Tw caused by the EtBr is converted to negative writhe (Wr), which is the physical consequence arising from the fact that the linking number (Lk) cannot be altered in covalently closed circular DNA.

Chapter 2: Variola Type IB DNA Topoisomerase - DNA Binding and Supercoil

Unwinding using Engineered DNA Minicircles

Introduction

The free energy stored in the form of negative DNA supercoils is essential for many genomic DNA transactions[44,105,106]. Topological strain and the associated DNA strand separation promotes initiation of DNA replication[6,107,108], RNA transcription[109-113], and facilitates homologous recombination[9]. In addition, because the free energy trapped within an entire DNA superhelical domain must be partitioned between twist and writhe, local unwinding events caused by protein binding or DNA strand breaks can be rapidly propagated over large distances within the domain by the associated changes in writhe. Such local events that bring about changes in the three-dimensional topology of DNA can promote interactions between bound proteins that would otherwise be separated by large distances in the linear DNA sequence, and they could also be used as a signaling event for DNA damage[19,114]. The above essential processes occur in all eukaryotic cells and rely on the maintenance of a steady-state level of DNA supercoiling regulated in part by type I DNA topoisomerase enzymes[35,115]. These catalysts serve to remove the excess supercoils generated during the cellular processes of DNA replication and transcription and allow the steady-state superhelical density to be optimally maintained[35].

Given the global importance of negative supercoiling, it is of interest to understand if eukaryotic type IB topoisomerases sense features of DNA superhelical topology. Such a mechanism could target these enzymes to highly supercoiled DNA domains and also preclude these abundant catalysts from completely unwinding genomic DNA. Type IB topoisomerases bind nonspecifically to DNA and form a C clamp structure that allows them to interact with the phosphate backbone of both strands of the DNA duplex, but these enzymes cause little overall distortion of the linear duplex structure[44,57,67]. Structural and mechanistic studies have not established whether type IB topoisomerases recognize superhelical nodes[73], bind more tightly to destabilized negatively supercoiled duplex structures[82], or detect other subtle features of supercoiled DNA in preference to relaxed DNA.

Although biased affinity for DNA of high superhelical density would be an attractive mechanism for targeting topoisomerases to where they are needed in the genome, it is not the only possible specificity mechanism. An attractive alternative would be for the enzyme to take advantage of the intrinsic structural or dynamic properties of supercoiled DNA *after* it has formed a covalent phosphotyrosyl linkage[35]. Since the lifetime of the covalent intermediate and the swivel rate of the mobile portion of the DNA determine the number of supercoils that are removed each time the enzyme cleaves DNA[53], this kinetic intermediate is especially well-suited to regulate supercoil unwinding. In this regard, both ensemble and single molecule measurements have established that type IB topoisomerases remove multiple supercoils each time a DNA strand is cleaved[53,54]. Moreover, the number of supercoils that are removed during the

lifetime of the covalent intermediate is influenced by interactions between the enzyme and the DNA and the intrinsic superhelical torque[54,58].

Specificity and efficiency for unwinding highly supercoiled DNA could be obtained in several ways that are related to the unwinding mechanism. First, the lifetime of the covalent intermediate could increase with higher superhelical density, resulting in a larger time window for DNA rotation for supercoils to be unwound. Second, the efficiency of supercoil unwinding could be enhanced in highly supercoiled DNA substrates due to faster duplex rotation resulting from the high superhelical torque that is present. Finally, the enzyme-DNA interactions that restrict rotation could be weaker in the context of a highly mobile DNA segment.

The above mechanistic questions have been difficult to address using standard plasmid supercoiled substrates because most type IB topoisomerases cleave DNA nonspecifically and each cleavage site has a different lifetime for the covalent intermediate and an unknown rate of supercoil unwinding. Here we describe the synthesis and characterization of plasmid minicircles that contain only a single cleavage site for the sequence specific topoisomerase from variola virus (vTopo). In addition to allowing the study of sequence specificity in the context of supercoiled DNA, these substrates can be supercoiled to different densities allowing mechanistic investigation of the effect of supercoiling and torque on enzyme activity. These engineered minicircles also have features that allow for the insertion of unnatural nucleotides containing base or backbone substitutions, which will foster further informative studies on topoisomerase action on supercoiled DNA.

Experimental Methods

Cloning, Expression, and Purification of vTopo. Wild-type vTopo was expressed in *E.coli* T7 Express cells and purified as previously described using phosphocellulose chromatography[116]. The K271E mutant vTopo was made in a similar manner and purified as described[58].

Minicircle Construction. A 1,000 bp sequence containing the 454 bp minicircle (MC^{sp}) sequence and flanked by NcoI and XhoI restriction sites was generated by gene synthesis (Integrated DNA Technologies) in the pIDTSMART-Amp vector. The 1,000 bp sequence was cloned into the 3,000 bp pattD vector using its NcoI and XhoI sites to produce pMC454 (Fig. 2.1)[97]. The size and sequence of pMC454 was confirmed via agarose gel electrophoresis and DNA sequencing (Fig. 2.2).

MC^{sp} Expansion in Bacteria, Disintegration and Decatenation. pMC454 was transformed into LZ54 cells via heat shock, conditioning, and growth at 30°C as previously described[97]. A 10 mL overnight culture grown in LB/Amp at 30°C was used to inoculate 350 mL of modified TB (12 g tryptone, 48 g yeast extract, 30 mL glycerol, 0.1 mL antifoam 204, 2.32 g KH_2PO_4, and 12.54 g K_2HPO_4 per liter). Inoculated media was incubated at 30°C with shaking at 225 rpm to an OD_{600nm} of 2.0. The culture was then heat shocked to induce λ-integrase activity via the addition of 350 mL of modified TB preheated to 60°C and cultures continued to shake at 42°C for 30 minutes before norfloxacin was added to a final concentration of 30 μg/mL. The temperature was returned to 30°C and cells continued to shake for one hour[97].

Cells were harvested via centrifugation at 6,000 x g for 15 minutes, resuspended in Buffer P1 (Qiagen), and frozen at -20°C. Plasmid DNA was purified using a HiSpeed

Maxiprep Kit (Qiagen) according to manufacturer's instructions and eluted into 1 mL Buffer EB (10 mM Tris-Cl, pH 8.5). To confirm that the λ-integrase disintegration reaction and decatenation was complete, 1 μL of eluent was run on a 1% agarose gel (Fig. 2.2).

MC^{sp} Purification. About 125 μg of eluted DNA was run on a 0.7 or 1% agarose gel to purify the MC from all other DNA. The band containing the desired MC product was excised following staining with EtBr and destaining with distilled water. MCs were gel extracted in one of two ways. In the first method, a Qiaquick Gel Extraction Kit (Qiagen) was used. In the second, the agarose gel slice was incubated for at least 24 hours in 3X (w/v) Gel Extraction Buffer (300 mM NaOAc, 1 mM EDTA) while shaking at 37°C to allow the DNA to diffuse out of the gel. Isolated MC^{sp} was concentrated with a Millipore concentrator (MWCO = 10kDa), buffer exchanged using a PCR Purification Kit (Qiagen), and eluted with distilled water. Concentrations were determined using a Nanodrop spectrophotometer with calculated extinction coefficients at 260 nm absorbance measurements. Purity was assessed using agarose gel electrophoreses (1% agarose) (Fig. 2.2).

Construction of MC^{ns}. A MC where the specific vTopo site was removed (MC^{ns}) was constructed from pMC454 using the following mutagenesis primers (altered nucleotides are in bold) to form pMC454I in a Quikchange Mutagenesis Kit according to manufacturer's instructions:

5'-CGGATCGCCTCAGCGAC**GA**TTATTCGGGTCGACGC-3'
3'-GCCTAGCGGAGTCGCTG**CT**AATAAGCCCAGCTGCG-5'

Mutations were confirmed by DNA sequencing. MC^{ns} was obtained by bacterial expansion of pMC454I and disintegration as described above for MC^{sp}. The identity of

MC^{ns} was confirmed using vTopo supercoil relaxation assays in addition to agarose gel electrophoresis to determine purity.

Construction of MC^{sp2}. Plasmid pMC1752 was designed to generate a larger 1,752 bp MC with a single vTopo recognition site (MC^{sp2}). pMC1752 was constructed using a 661 bp sequence of DNA constructed via gene synthesis (Integrated DNA Technologies) (Fig. 2.3). This sequence contains no specific vTopo recognition sites and no other pentapyrimidine sequences. The 661 bp sequence was cloned out of the IDT vector and into phosphatase-treated pMC454 using PstI sites to create pMC1103. The identity of pMC1103 was confirmed by agarose gel electrophoresis. pMC1103 contains a NheI site between the two PstI sites, in the 661 bp sequence segment that was inserted, and this site conflicts with subsequent cloning strategies. Therefore, it was removed by mutagenesis before the second round of cloning to form pMC1752 from pMC1103 with the following mutagenesis primer (mutated positions are in bold):

5'-CCAGGCTATGATAGAATG**AG**AGCCTGCAGTAAGCTTTACCTGAGC-3'

In the second round of cloning, the 661 bp sequence was cut out of the IDT vector using NheI sites (rather than the PstI sites used above) and ligated into NheI-digested pMC1103 that had been pretreated with phosphatase to create pMC1752. The identity of pMC1752 was confirmed via 1% agarose gel electrophoresis. Following confirmation, pMC1752 was expanded and MC^{sp2} was obtained as stated above for MC^{sp}. The identity of MC^{sp2} was confirmed using vTopo activity assays in addition to agarose gel electrophoresis to determine its purity.

Ethidium Bromide Supercoiling of Minicircles. Intercalating agents such as ethidium bromide (EtBr) can be used to introduce negative supercoils into circular DNA[117]. This

is accomplished by creating a transient nick in the DNA backbone in the presence of EtBr, resealing the backbone, and then removing the EtBr to restore the native twist of the DNA[103]. Purified MC^{sp} and MC^{ns} were supercoiled by reacting 10 nM of each MC with 100 nM vTopo in the presence of 1.5 µg/mL EtBr for one hour to make MC^{sp*} and MC^{ns*}. Following incubation, EtBr was removed via two rounds of phenol-chloroform extraction and the MCs were purified using two PCR Purification Kits (Qiagen). After the second column, each MC was eluted with distilled water and the concentration was determined using a Nanodrop spectrophotometer. Supercoiling and purity of each MC was ascertained using electrophoresis through a 5% native polyacrylamide gel (19:1) in the presence of TBM Buffer (90 mM Tris, 90 mM Boric Acid, 10 mM MgCl$_2$) at 4 W for 6 hours or 1 W overnight (Fig. 2.4, rightmost lane). Gels were stained with SYBR Green (Life Technologies) for 30 minutes and imaged using a Typhoon imaging system (GE Healthcare).

Superhelical Density and Linking Number Determinations. To determine the linking number and superhelical density of MC^{sp}, MC^{ns}, and MC^{sp*} electrophoresis was performed using a 6% native polyacrylamide gel (75:1) containing chloroquine concentrations between 1 and 20 µg/mL. The running buffer was 1X TBE (90 mM Tris Base, 90 mM Boric Acid, 2 mM EDTA) containing the same concentration of chloroquine. Electrophoresis was performed for 18 hours at 3 V/cm (Fig. 2.5)[118]. A similar process was used to determine the number of supercoils present in MC^{sp2} except that 2% agarose gels containing chloroquine concentrations between 1 and 5 µg/mL were used. Electrophoresis was performed for 18 hours at 4 V/cm in the cold room using TAE Buffer (40 mM Tris Base, 20 mM acetic acid, 1 mM EDTA) containing the

same concentration of chloroquine. (Fig. 2.6). Gels were stained with SYBR Green and imaged.

Following imaging, the number of supercoils present in each MC was determined[102]. First the bands in each gel lane corresponding to the topoisomer distribution generated at a given chloroquine concentration were fitted to Gaussian peak shapes using the QuantityOne software. Bands with identical intensities with different chloroquine concentrations were aligned to allow reliable counting of linking number differences. All intensities were then plotted against the number of negative supercoils they contained and fit to a Gaussian distribution to determine the mean number of negative supercoils and standard deviation (Table 1, Fig. 2.5 and 2.6)[102]. Once the average number of supercoils was determined, the superhelical density (σ) was calculated using eq 1.

$$\sigma = \frac{-10.5 \frac{\text{bp}}{\text{turn}} \text{ x Average Number of Supercoils}}{\text{DNA Length in bp}}$$

(1)

Competition Binding Experiments. A fluorescein (FAM) fluorescence-based continuous steady-state DNA vTopo cleavage assay was performed as described in Kwon, et al.[4,105], except that the Dabsyl quencher was replaced with Iowa Black (IABK, IDT). Briefly, the 18U-FAM/18-IABK ribonucleotide substrate was annealed in Buffer A (20 mM Tris, pH 9, 200 mM NaCl) overnight using 110 μM 18U-IABK strand and 100 μM 18U-FAM strand. One micromolar of the ribonucleotide substrate and various concentrations of competitor DNAs were combined in 148 μL Buffer A. The sample was placed into a Quartz microcuvette (0.3 cm, Starna Cells) at 37°C and readings were taken every 15 s for 5 to 10 minutes at an excitation wavelength of 492 nm and an emission wavelength

31

of 522 nm with an integration time of 2 s in a fluorometer (Fluoromax-3). Excitation

slits were set at 0.5 nm and emission slits were at 7 nm. Following the initial scan, 1.5

μL of 1 μM vTopo was added to the cuvette to give a final concentration of 10 nM and

the increase in fluorescence intensity was monitored continuously after a 30 s

equilibration period. Readings were taken every 15 s for at least 135 s in triplicate.

Time courses were fit to a linear regression line in Prism (Graphpad).

Corrections were made for the background fluorescence at 522 nm. The fluorescence

change at each time (F_t - F_0) was converted to percent reaction by normalization to the

maximum fluorescence change (F_{max} - F_0) corresponding to complete reaction for the

substrate according to eq 2 (Fig. 2.7):

$$\% \text{ Reaction} = \frac{F_t - F_0}{F_{max} - F_0} \text{ x } 100$$

(2)

The K_i for each competitor (in bp) was calculated using equation 3 using the known K_m

= 7920 nM bp and [S] = 18000 nM bp[54,105]:

$$\frac{v}{v_o} = \frac{[S] + K_m}{K_m \left(1 + \frac{X}{K_i}\right) + [S]}$$

(3)

The competitor DNAs used in these experiments were MC^{ns}, linearized MC^{ns}

(MC^{nsL}), MC^{ns*}, a nonspecific 206mer, and a nonspecific 35mer. The construction of

MC^{ns} and MC^{ns*} is described above. MC^{nsL} was obtained by digestion with PstI-HF and

the nonspecific 206mer was constructed by PCR using pMC454I as the template and

had the following sequence. The underlined portion represents the region to which

primers were annealed (IDT):

GCAGATACTCACCTGATGACTGAACGGATCGCCTCAGCGACGATTATTCGGG

TCGACGCTACCTCAGCAGCGATGCTAATGATGTCGATAGTTACTAACGGGTC

ATTGTTCGATTAACTGCCGCAGCAACATCAGGCACCAGTAGCGTGGGCGTAA

ACAGTAGTGTTACCAGGATGGCGAGCTTAGCAGTCGGTAAACCTGTCGTG

The nonspecific 35mer was obtained by annealing the mutagenesis primers that were used for construction of MC^{ns} (see above). All constructs were confirmed by gel electrophoresis. To account for differences in DNA length, we express binding in base pair molarity and not molar concentration of the DNA molecules.

Single-Turnover Kinetics. Ten nanomolar MC^{sp} or MC^{ns} was reacted with 20, 40, or 80 nM vTopo in a single 80 μL reaction in supercoil release buffer (50 mM Tris, pH 7.5, 100 mM NaCl, 1 mM DTT, 20 μg/mL BSA, 0.01% Brij-35, 5 mM MgCl$_2$) by adding 40 uL 2X vTopo to 40 uL of 20 nM MC with vigorous mixing. At desired time points (Figs. 2.18 and 2.19), 10 μL were removed from the reaction and added to 10 μL of 2X quench buffer (1% SDS, 20% glycerol in 1X Tris-glycine). Fifteen microliter of the quenched reaction was loaded onto a 2% agarose gel run in 1X TAE for 1 hour at 100 V. Gels were stained for 10 minutes with 0.5 μg/mL EtBr and destained with distilled water before being imaged. All experiments were performed in triplicate.

Gels bands were quantified using Quantity One software (Biorad) and areas were determined by nonlinear least squares fitting to Gaussian peak shapes. Due to unequal EtBr staining between the relaxed and supercoiled bands on agarose gels, the raw fluorescence of the relaxed product bands were multiplied by a normalization factor of 1.4 obtained from a standard curve (Fig. 2.8). Following normalization, the concentration of product at each time ([P]$_t$) was calculated according to equation 4

where F_p represents the normalized fluorescence of the product and F_s the fluorescence of the substrate.

$$[P]_t = \frac{F_p}{F_p + F_s} \times [S_0]$$

(4)

The time courses for product formation were fit to a first-order rate equation (Graphpad Prism). The assumption of pseudo first-order kinetics was confirmed using *Dynafit 3* (Biokin).

Steady-State Kinetics. Steady-state kinetic experiments were performed similarly to those described above for single turnover conditions, including the quantification of gel images and normalization for the product species fluorescence. In these experiments, 2.5, 5 or 10 nM MC^{sp} or MC^{ns} were reacted with 1 nM vTopo in an 80 µL reaction volume. The slope of the initial linear rates was used to determine v_{max}.

Supercoil Unwinding Mechanism of MC^{sp}, MC^{sp*} and MC^{sp2}. All reactions to investigate the kinetics of supercoil unwinding were performed in supercoil release buffer by adding 2X vTopo (WT or K271E) to 2X MC to achieve a final concentration of 5 nM DNA and 5 nM enzyme. Reactions were carried out for desired times and 10 µL samples were removed and quenched by adding 10 µL of quench buffer. For MC^{sp} and MC^{sp*}, 30 µL of distilled water was added to each quenched time point followed by extraction with phenol/chloroform twice. Samples were dried under vacuum and resuspended in 10 µL distilled water and 2 µL 6X loading dye before loading 6 µL onto a 6% native PAGE gel (75:1 acrylamide:bis) in 1X TBE. Gels were run for 18 hours in the cold room at 4 V/cm. For MC^{sp2}, no further manipulation was necessary. An 8 µL reaction sample was loaded onto a 3% agarose gel and then run in 1X TAE buffer in the cold room for 24

hours at 3 V/cm. All gels were stained for at least one hour with SYBR Green and imaged using a Typhoon imaging system.

Bands were quantified using Quantity One software with the Gaussian peak shape fitting routine. The measured Gaussian peak areas were used to determine the molar amounts of each band at each time point in the supercoil unwinding reaction. Standard curves were used to confirm that there were no staining differences between different topological forms of DNA (Fig. 2.9 and 2.10). To account for possible inconsistencies in staining across the gel and loading of the lanes, all bands were quantified as a fraction of the total DNA loaded in a lane. The molar concentration of each species was calculated by multiplying the fractional contribution of an individual band by the total concentration of substrate. If necessary, the amount of nicked DNA initially present in the substrate was subtracted from overlapped product bands. All reactions were performed in duplicate.

Kinetic Simulations of Supercoil Unwinding. The data were fitted by numerical integration methods using *Dynafit 3*. The Dynafit input script files are found in Fig. 2.11-2.14.

The definitions of the kinetic constants are listed below.

k_{lim} - the rate limiting intramolecular rate constant representing all steps prior to the supercoil unwinding process. This rate constant is given directly by the exponential decay rate of the substrate topoisomers. This step is considered irreversible because of the rapid removal of supercoils from the cleaved substrate and the observation that the most highly supercoiled substrate topoisomers do not relax into other substrate topoisomers with lesser supercoils (Fig 2.15).

k_{cl} – the chemical step of cleavage. In the models, this is fixed at 0.3 s^{-1} for WT vTopo based on previous experiments with small oligonucleotides and the pUC19 plasmid[53,67]. The cleavage rate is only relevant when intermediates react because the enzyme is already positioned at the specific site (i.e. rate-limiting translocation obscures cleavage in the reaction of substrate topoisomers).

k_{lig} – the chemical step of ligation. In the models, this rate is fixed at 4 s^{-1} for WT vTopo based on previous experiments with small oligonucleotides and the pUC19 plasmid[53,54]. For intermediates with low superhelical density, ligation competes effectively with supercoil unwinding. The ratio between rate of unwinding and ligation determines the number of supercoils released per cleavage event. It also influences the overall rate at which product formation takes place from intermediates (i.e. under conditions of rapid equilibrium cleavage/ligation followed by slow supercoil unwinding).

$k_{s \to p}/k_{s \to i}$ – the ratio of the rates of product and intermediate formation arising from cleavage of the substrate pool. Because k_{lim} is the rate-limiting step in substrate disappearance, the individual values for the rapid steps $k_{s \to p}$ and $k_{s \to i}$ are not measured (i.e $k_{s \to p}$ and $k_{s \to i} \gg k_{lim}$). However, the amount of intermediates and product, which are generated from a common cleaved substrate pool, accurately reveals the ratio $k_{s \to p}/k_{s \to i}$. It is important to note that $1/k_{s \to i}$ includes (i) the unwinding time to produce an intermediate with Δn fewer supercoils, and (ii) the time required for ligation. Therefore, the lower limit time for $k_{s \to i}$ is $1/k_{lig}$ $= 1/4 \text{ s}^{-1} = 0.25 \text{ s}$.

$k_{i \to p}/k_{lig}$ - the ratio of product formation from intermediate pools as compared to the ligation rate. As above, we assign a ligation rate of 4 s^{-1}.

We sought the simplest kinetic model to describe the data. We began with complex models and then performed step-by-step simplification to arrive at the models used. The details of these simplifications and any assumptions that were used are described below.

<u>MC^{sp}.</u> For this substrate, two substrate populations $s^{-2,-3}$ and s^{-1} existed (Fig. 6B). There was no observable intermediate formation, as the disappearance of $s^{-2,-3}$ followed a single exponential decay to product with rate constant k_{lim} without populating s^{-1}. Thus, there is no information of partitioning between intermediates and product with this substrate. Due to its single supercoil, topoisomer s^{-1} could only proceed to product. Since s^{-1} disappeared more slowly than $s^{-2,-3}$ and the chemical steps of cleavage and ligation are known to be similar in linear and supercoiled substrates, the slower rate is most reasonably attributed to rapid equilibrium cleavage and ligation followed by slow unwinding of this topoisomer because of its low superhelical density ($k_{s-1 \to p}$). We assigned k_{cl} and k_{lig} as above, and report the ratio $k_{s-1 \to p}/k_{lig}$ in Table 2.

<u>MC^{sp*}.</u> For this substrate, a single intermediate (i^{-1}) accumulates. The $s^{-4,-5,-6}$ substrate pool followed a single exponential decay and there is no evidence that $s^{-4,-5,-6}$ partitions into another substrate band. Thus, the substrate pool was treated in the same way as described above for $s^{-2,-3}$ to give k_{lim}. Since the decay of $s^{-4,-5,-6}$ resulted in both product and the i^{-1} intermediate, the ratios $k_{s \to p}/k_{s \to i}$ and $k_{i \to p}/k_{lig}$ could be determined. Trial and error simulations demonstrated that these ratios were invariant as long as $k_{s \to p}$, $k_{s \to i}$, and k_{lig} were much greater than k_{lim}. We assigned k_{cl} and k_{lig} as above, and report the ratios $k_{s \to p}/k_{s \to i}$, $k_{s-1 \to p}/k_{lig}$ in Table 2.

MC^{sp2}. For this substrate, five intermediates accumulate and then disappear into product bands. As above, the substrate was treated as a single pool that followed a single exponential decay to product and intermediates (see justification of this simplification in Figure S8). With the accumulation of multiple intermediates, it was also important to confirm whether more highly supercoiled intermediates relaxed into intermediates with lower superhelical densities. Using the same procedure outlined for the substrate topoisomers (Figure S8), we were able to discern two populations of intermediates (I1 and I2) that behaved distinctly. Pool I1 consisted of $i^{-5,-6.-7}$ with each member of the pool appearing and disappearing with similar rates. Pool I2 consisted of $i^{-2,-4}$ which appeared and disappeared with a similar rates but more slowly than I1.

K271E mutant vTopo. The model for K271E and the MC^{sp2} substrate was obtained using the same procedures described above for WT vTopo. The value for k_{lim} was obtained directly from the rate of disappearance of the substrate pool. However, i^{-1} was classified as a product because it did not disappear with time, and accordingly, it was pooled with the product bands. It is likely that i^{-1} eventually disappears over a longer time, but this was not observable because of the slow cleavage rate of the K271E mutant[44,58]. This treatment of the i^{-1} species does affect the data analysis because very few intermediates accumulate with K271E. For K271E, k_{cl} and k_{lig} were set 20-fold lower than the WT enzyme based on previous results with linear substrates[54,58]. Although it is possible that these calculated values are not precise, the ratio $k_{s\rightarrow p}/k_{s\rightarrow i}$ is completely independent of any assumptions. Therefore, the major conclusion that fewer intermediates accumulate with K271E is also independent of assumptions.

Results

Minicircle Design, Purification, Supercoiling, and Linking Number Determination. An efficient technology for minicircle synthesis has recently been reported that uses *in vivo* integrase activity on plasmids having integrase recombination sites in direct orientation[97,119]. Taking advantage of this technology, a custom minicircle sequence was designed that contained a single vTopo recognition site (5'-CCCTT-3') and no other similar pentapyrimidine sequences (Fig. 2.2). The sequence was incorporated into a plasmid containing the bacteriophage λ-integrase sites attB and attD in direct orientation to allow disintegration of the MC upon transformation of strain LZ54[97]. Upon successful disintegration and decatenation, two circular DNA molecules consisting of the MC and a larger circle containing the accessory elements necessary for growth and replication were obtained (Fig. 2.2). The minicircle was successfully purified, yielding between 5 and 10 μg MC per 350 mL bacterial culture depending on the MC size.

The 454 bp minicircle containing a single recognition site (MC^{sp}) was visualized using atomic force microscopy and consisted of topological forms with a mean of 2.7 negative supercoils (SD = 1.1), corresponding to an average superhelical density of -0.057, which matches the expected superhelical density of closed circular DNA isolated from *E. coli* cells[97,119,120]. The superhelical density of MC^{sp} was increased beyond this basal level using reversible strand nicking by vTopo in the presence of EtBr to make MC^{sp*} (Fig. 2.4). Highly supercoiled MC^{sp*} was optimally generated using 1.5 μg/mL EtBr and contained an average of 5.4 negative supercoils (SD = 1.7), corresponding to an average superhelical density of -0.125 (twice that of MC^{sp}). Although all MCs migrated as single bands during agarose gel electrophoresis, they consisted of a

Gaussian distribution of topoisomers when electrophoresis was performed using 5% polyacrylamide gels in the presence of 10 mM $MgCl_2$, or using a 6% native gel in the presence of chloroquine (Fig. 2.4 and 2.5)[53,58,97]. The 454 bp minicircle that lacked the specific site (MC^{ns}), as well as its corresponding highly supercoiled form MC^{ns*}, followed the same topological distributions as MC^{sp} and MC^{sp*}.

We also prepared a larger 1,752 bp minicircle with a specific site (MC^{sp2}). Using agarose gel electrophoresis in the presence of chloroquine, we determined that MC^{sp2} isolated from cells had an average superhelical density of about -0.067 and a Gaussian topoisomer distribution with a mean of 11.2 negative supercoils (SD = 1.4) (Fig. 2.6).

DNA Topology does not Impact vTopo Nonspecific DNA Binding Affinity. In the absence of unreactive supercoiled substrates, it has not been previously possible to study the contributions of DNA topology to the nonspecific binding affinity of vTopo[51]. Using a continuous fluorescence steady-state kinetic assay we measured the inhibition of DNA cleavage by vTopo using various competitor DNAs that lacked the specific 5'-CCCTT-3' site. In this assay[105], the action of vTopo causes a linear time dependent increase in fluorescence intensity as DNA strand cleavage releases a FAM-labeled 7mer strand (Fig. 2.16A and 2.16B). As the concentration of supercoiled MC^{ns} competitor DNA was increased from 0 to 10 nM, the rate of cleavage of the reporter substrate was completely inhibited (Fig. 2.16C). In addition to MC^{ns}, this assay was used to test the inhibitory potentials of MC^{nsL}, MC^{ns*} (ρ = -0.125), and shorter lengths of linear nonspecific DNAs (Fig. 2.16D). Control experiments showed that MC^{ns} was not relaxed by vTopo over the course of these competition binding measurements (Fig. 2.17).

For supercoiled MC^{ns} (ρ = -0.057), we detected tight binding with a K_i of 167 ±

47 nM bp. Linearized MC^{nsL} and highly supercoiled MC^{ns*} were found to compete

similarly, with K_i values of 310 ± 50 nM bp and 240 ± 50 nM bp, respectively. Thus,

there is no evidence that DNA topology significantly impacts nonspecific DNA binding

by vTopo. In contrast, the length of the competitor DNA was very important. While an

identical base pair concentration of a nonspecific 35mer competed poorly, an equivalent

concentration of a nonspecific 206mer had an intermediate competitive capacity (K_i =

4.5 ± 1 μM bp) (Fig. 2.16D). Since vTopo forms a C-clamp around duplex DNA[121],

these findings are most likely attributed to facilitated diffusion of the enzyme on longer

DNAs and the additional possibility of enhanced capture of the clamp on circular DNA,

which does not possess free ends for escape. Neither of these interaction modes are

possible with short oligomers.

Site-Specific Cleavage Kinetics of MC^{sp}. The presence of multiple vTopo recognition

sites on plasmid DNA substrates has hindered a quantitative understanding of DNA

cleavage because each site has a different rate constant for cleavage and ligation[53].

Using MC^{sp}, we now have the opportunity to measure vTopo cleavage of a single,

defined specific site in supercoiled substrates (Fig. 2.18A). In these measurements, we

found that the overall rate of DNA relaxation was limited by cleavage or a non-chemical

step that preceded cleavage. This step is represented by the single irreversible rate

constant (k_{lim}) that leads to the covalent complex E-MC^{sp} in Figure 2.18A (the

assumption of irreversibility is justified by the rapid rate of supercoil unwinding that

follows cleavage, as described below).

For MC$^{\text{sp}}$ with few superhelical turns, we expected that the substrate would be directly converted to product because ligation cannot effectively compete with supercoil unwinding when only a few supercoils are present (i.e. no partially relaxed topoisomer intermediates were expected). This expectation was confirmed in single turnover measurements using excess enzyme, where substrate was directly relaxed to product in a single-exponential manner (Fig. 2.18B). We observed a linear concentration dependence of k_{lim} for MC$^{\text{sp}}$, corresponding to a second-order rate constant of $k_{\text{lim}}' = 1.7 \times 10^6 \text{ M}^{-1}\text{s}^{-1}$ (Fig. 2.18B). The largest accessible k_{lim} was 0.15 s^{-1} at 80 nM vTopo. This value may be compared with the previously measured concentration *independent* $k_{\text{lim}} = 0.3$ s^{-1} for pUC19, a plasmid that contains 17 vTopo specific cleavage sites[53].

The concentration dependent rate of cleavage of MC$^{\text{sp}}$ was intriguing given the opposite result obtained with the multiple site plasmid. Since the binding measurements indicate exceedingly tight DNA binding (Fig. 2.16), the concentration dependence for MC$^{\text{sp}}$ could not be attributed to a simple increase in the concentration of the ES complex as the enzyme concentration was increased; under the conditions of these experiments each MC DNA was saturated with one or more enzyme molecules (E$_n$•MC$^{\text{sp}}$, Fig. 2.18A). Accordingly, the concentration dependence for MC$^{\text{sp}}$ must arise from rate-limiting movement of the vTopo C clamp along the DNA until its recognition sequence is encountered[67]. As more vTopo molecules are added, the probability of finding the cleavage site increases linearly because more enzyme molecules (*n*) are scanning each substrate molecule for the single recognition site (E$_n$•MC$^{\text{sp}}$, Fig. 2.18A). For pUC19, the problem of finding a site is lessened because a recognition site is present at an average density of about one in every 150 bp of DNA[44,51,53,120,122].

We also measured initial rates for reaction of MC^{sp} under steady-state conditions (Fig. 2.18C). Using three different substrate concentrations in the range 2.5 to 10 nM, we found that the rate constant was concentration *independent* (0.02 s^{-1}), providing an upper limit estimate for the K_m (MC^{sp}) $\leq$ 0.5 nM (Fig. 2.18C). The low K_m value is consistent with the low K_D for nonspecific DNA binding and supports the above contention that concentration dependence of the single-turnover reaction of MC^{sp} arises from multiple enzyme molecules performing an intramolecular transfer step.

Cleavage Kinetics of Nonspecific Minicircle (MC^{ns}). It is known from DNA cleavage studies using small duplex oligomers that the specific 5'-CCCTT-3' pentapyrimidine sequence is required for vTopo activity[51]. Using MC^{ns}, we sought to determine whether a specific sequence was equally important for cleavage of a supercoiled substrate. Although the time dependent cleavage was much slower for MC^{ns} as compared to MC^{sp}, it was easily detectable because rapid supercoil unwinding efficiently traps rare cleavage events (Fig. 2.19A). Single-turnover rates were concentration dependent as observed for the specific substrate, but the apparent second-order rate constant $k_{lim}' = 5.9 \times 10^4$ M^{-1}s^{-1} was reduced by 30-fold (Fig. 2.19A, inset). As a point of comparison we note that this apparent sequence specificity of vTopo is much less than that of restriction enzymes $(10^5$-$10^6)$[123].

Under limiting enzyme steady-state conditions, we were able to measure an observed rate constant of 3.7×10^{-4} s^{-1} using 1 nM vTopo and 2.5 nM MC^{ns}, which is ~50-fold less than MC^{sp} under the same conditions (Fig. 2.19B). Further steady-state measurements were not possible because higher concentrations of MC^{ns} proved inhibitory to the reaction. This inhibition is likely due to significant substrate inhibition.

Thus under limiting enzyme conditions, the apparent specificity of vTopo increases as the [S]/[vTopo] increases.

Supercoil Unwinding of MC^{sp}, MC^{sp*} and MC^{sp2}. To explore whether supercoil unwinding proceeds through the generation of topoisomer intermediates, we extended the relaxation experiments to MCs that contained increasing numbers of supercoils. The expectation was that highly supercoiled substrates would provide a greater opportunity for detection of intermediates because the finite probability for strand ligation increases with the number of unwinding events needed to reach relaxed product (Fig. 2.20A).

Unlike previous supercoil unwinding studies using the multiple site substrate pUC19 under conditions of excess enzyme[53,58], the present studies were performed with a [E]/[DNA] ratio of ~1 and concentrations of enzyme and DNA that exceeded the estimated K_D value by at least 10-fold. Therefore, the DNA is saturated with enzyme and the rate-limiting step (k_{lim}) reflects an intramolecular event leading to site-specific cleavage. Accordingly, the rate constants for rapid steps that follow cleavage (unwinding and ligation) are not revealed in these kinetic measurements. However, the measurements robustly report on partitioning of the initial substrate pool (*s*) between complete unwinding to form product (*p*) or partial unwinding with ligation to form topoisomer intermediates (*i*). Partitioning is quantified by the ratio $k_{s \rightarrow p}/k_{s \rightarrow i}$ (Fig. 2.20A), which is the key descriptor reflecting the average number of supercoils that are unwound before a ligation event traps a topoisomer intermediate. Since cleavage is rate limiting, topoisomer intermediates that accumulate must react in subsequent cleavage/ligation events that ultimately yield relaxed product ($k_{i \rightarrow p}$). For topoisomer intermediates with lower superhelical torques, the assumption of irreversible cleavage

followed by rapid unwinding was not appropriate. Accordingly, the model in Figure 2.20A allows for ligation of cleaved intermediates (k_{lig}), which can compete with the unwinding step ($k_{i \rightarrow p}$). Thus, multiple rounds of cleavage (k_{cl}) and ligation are allowed before a successful unwinding event to give product.

The expectation that intermediates would be detected with more highly supercoiled MCs was borne out when the relaxation of MC^{sp*} (mean = 5.4 negative supercoils) was compared with MC^{sp} (mean = 2.7 negative supercoils) using high-resolution polyacrylamide gel electrophoresis to resolve topoisomers. Consistent with the above results using low-resolution agarose gel electrophoresis (Fig. 2.18), the unwinding of MC^{sp} did not generate any observable topoisomer intermediates (Fig. 2.20B). However, we did resolve a minor substrate topoisomer (s^{-1}) with one negative supercoil that relaxed much more slowly than the more highly supercoiled substrate topoisomers ($s^{-2,-3}$) (Fig. 2.20B, Table 1). We attributed the slower relaxation rate of s^{-1} to its reduced superhelical torque, which would reduce the driving force for progressing forward to relaxed product ($k_{s-1 \rightarrow p}$)[54,124]. Our attribution of this effect to $k_{s-1 \rightarrow p}$ (and not k_{cl} or k_{lig}) is supported by previous observations that cleavage (k_{cl}) and ligation (k_{lig}) are similar in linear and supercoiled substrates[51,53,58,71,97]. Thus topoisomer s^{-1} disappears more slowly because it spends more time undergoing repetitive cycles of cleavage and ligation before a productive unwinding event occurs. Similarly, MC^{sp*} showed a slowly relaxing intermediate (i^{-1}) that contained a single negative supercoil. An intermediate defined as a distinct topoisomer not present in the initial substrate pool that is observed to accumulate and then proceed to product over time (Fig. 2.20C). The simulations of these two data sets led to the rate constants reported in Table 2 and discussed further

below. Qualitatively, these data demonstrate that ligation is poorly competitive with supercoil unwinding when 5-6 supercoils are present in the starting substrate topoisomer pool, but not when 2-3 supercoils are present. Another salient point is that ligation can efficiently compete with unwinding under conditions of low superhelical density.

We extended the investigation to a larger minicircle (MC^{sp2}) that contained 1,752 bp and an average of 11.2 negative supercoils (Fig. 2.21). With MC^{sp2}, the substrate topoisomers s^{-14} to s^{-9} were overlapped in a normal 3% agarose gel, but all other topoisomer species generated during relaxation were resolved. The situation of overlapped substrate bands required confirmation that relaxation of the most highly supercoiled substrate topoisomers did not generate relaxed topoisomers that overlapped with other substrate topoisomers (e.g. s^{-14} did not relax to form $s^{-9 \text{ to } -13}$). This point was established using a chloroquine gel that resolved substrate bands, which were observed to disappear at a uniform rate into resolved intermediate topoisomers and not other substrate topoisomers (Fig. 2.15). Thus, the entire substrate pool comprised of s^{-14} to s^{-9} can be economically treated as a single species in the kinetic analysis (Fig. 2.21A).

While supercoil unwinding of MC^{sp^*} went through a single detectable intermediate (Fig. 2.20C), we now observed five intermediates that accumulated and then disappeared during relaxation of MC^{sp2} ($i^{-2 \text{ to } -7}$, Fig. 2.21B). As shown in the kinetic model in Figure 16A, these intermediates were divided into two pools consisting of $i^{-5 \text{ to } -7}$ (pool I1) and $i^{-2, -4}$ (pool I2). This simplification was justified because all of the intermediates within each pool appeared and disappeared with equal rates, and pool I1 proceeded directly to product ($k_{I1 \to p}$) without generating detectable amounts of pool I2 intermediates. The maximal level of pool I1 was less than pool I2, which is accounted

for by the different ratios $k_{s\rightarrow p}/k_{s\rightarrow I1} = 3.8 \pm 0.26$ and $k_{s\rightarrow p}/k_{s\rightarrow I2} = 2.1 \pm 0.22$ for formation

of the pools, as well as the different partitioning ratios to form product $k_{I1\rightarrow p}/k_{lig} = 0.0084$

$\pm$ 0.0013 and $k_{I2\rightarrow p}/k_{lig} = 0.0032 \pm 0.00026$. The lower partitioning ratios for pool I2,

which has a lower average superhelical density than pool I1, is consistent with more

efficient capture and ligation of the rotating DNA segment as superhelical torque is

decreased. In other words, for pool I2, more rounds of cleavage and ligation occur

before a successful unwinding event generates product.

In summary, pool I2 accumulates to a greater extent than I1 for two reasons.

First, it takes more time to unwind the initial substrate supercoils to generate pool I2

intermediates (i.e. ΔLk is greater), which in turn increases the opportunity for a

successful ligation event. Also, the reduced unwinding torque for intermediates with the

superhelical densities contained in pool I2 allows for more efficient strand ligation. The

optimal fitted curves for wild-type vTopo are shown in Figure 2.21B and the optimized

rate constants are reported in Table 2.

Supercoil Unwinding by K271E vTopo. Previous studies indicated that cationic residues

on vTopo interact with the negatively charged DNA backbone of the rotating DNA

segment and impact the number of supercoils that are released per cleavage

event[51,54,58,59,87]. A previously characterized vTopo mutant (K271E) was known to

increase the number of supercoils that were removed per cleavage event and was a

desirable mutant to test using MC[sp2] [35,58,105]. Indeed, relaxation experiments with MC[sp2]

showed slower cleavage and fewer intermediates with K271E as compared to wild-type

vTopo (compare Fig. 2.21B and 2.21C). The numerical simulations indicated that the

probability of completely unwinding the substrate pool by K271E was increased as

compared to wild-type vTopo (K271E; $k_{s\rightarrow p}/k_{s\rightarrow I1} = 7.7 \pm 1.5$ and $k_{s\rightarrow p}/k_{s\rightarrow I2} = 15.1 \pm 5.1$), but unwinding of the two intermediate pools was similar (K271E; $k_{I1\rightarrow p}/k_{lig} = 0.017 \pm 0.0094$ and $k_{I2\rightarrow p}/k_{lig} = 0.013 \pm 0.017$). The increased substrate partitioning ratio for K271E as compared to WT vTopo suggests potential roles for this interaction. This mutation could result in less efficient capture of the rotating DNA segment, an increased lifetime of the covalent phosphotyrosyl intermediate (lower k_{lig}), and/or suboptimal positioning for strand ligation when high superhelical torque is present.

Discussion

DNA Topology and vTopo Binding. The superhelical density of DNA could influence the topoisomerase reaction at one or more steps along a reaction coordinate that involves DNA binding, site recognition, strand cleavage/religation and supercoil unwinding. In this regard, human type IB topoisomerase (hTopo) has been suggested to sense DNA topology and localize to regions of increased superhelical density or node regions where double helices cross themselves[73,79]. Using two nonspecific 454-bp substrates with varying levels of superhelical density, as well as the corresponding linear sequence, we found no topological dependence of nonspecific DNA binding to vTopo (Fig. 2.11 and Table 2.1). Although previous studies using very high vTopo to DNA ratios detected cooperative protein interactions that resulted in DNA synapse formation[81,82], such interactions were minimized in our competitive binding studies because of the very low concentration of free enzyme and the use of [DNA]$^{\text{free}}$/[protein]$^{\text{free}}$ much greater than one. Therefore, the dissociation constants reflect single enzyme binding events.

Binding to superhelical DNA nodes would be facilitated by the presence of a secondary DNA binding site on vTopo. For hTopo, such a site was localized to a linker

region and solvent-exposed basic residues in its core subdomain III[79]. Although the linker element is absent from the vTopo enzyme structure, its C-terminal catalytic domain contains the same conserved basic residue motif[67,92,121]. In one study, these residues were mutated on vTopo, resulting in disruption of plectonomic supercoiling where two duplexes bind to multiple vTopos and intertwine in a right-handed helix[53,84,86]. We do not expect that this weak DNA binding site is relevant under the conditions of our experiments for the above stated reasons. Instead, the weak site likely becomes important during DNA synapsis, taking advantage of an avidity effect when multiple vTopo molecules act cooperatively[82,84].

Topological Effects on DNA Strand Cleavage in Single Site MCs. Although previous studies with supercoiled pUC19 provided no evidence that DNA strand cleavage was enhanced by DNA supercoiling as compared to the rates observed with small DNA duplexes[53], we wanted to explore this explicitly using single site MCs. Using MC^{sp} with superhelical densities of –0.062 and –0.125 (Table 2.1), we observed a 3-fold *decrease* in the cleavage rate for the more supercoiled substrate. Although it would be tempting to conclude that increased DNA supercoiling reduced the cleavage rate, this interpretation is confounded by the additional observation that the single-turnover cleavage/relaxation reactions were enzyme concentration dependent. This concentration dependence was unexpected because direct DNA binding affinity measurements established that all vTopo molecules were saturated with MC's (Fig. 2.11). Similarly, the steady-state rates were saturable with low nanomolar concentrations of DNA (Fig. 2.13C). Thus, the concentration dependent single-turnover rates must be attributed to a concentration dependent *intramolecular rate-limiting step that precedes DNA cleavage*.

We surmise that in the case of excess enzyme over DNA, increasing the number of bound enzyme molecules increases the probability that a vTopo C clamp will find the cleavage site. Due to this slow intramolecular process, the DNA strand cleavage step is not directly observed with these MC's.

Rate-limiting intramolecular transfer should result in slower apparent cleavage rates for larger single site substrates such as MC^{sp2} because of the greater amount of nonspecific decoy DNA. Although MC^{sp2} does show a cleavage rate that is 50% that of MC^{sp}, this is less than their size ratio in base pairs (MC^{sp2}/MC^{sp} ~ 4). The lack of a direct proportionality between rate and size could result from DNA supercoiling, which serves to compact MC^{sp2} and lessen the volume that must be searched by intramolecular "hopping" steps. A further understanding of these aspects of the vTopo site recognition mechanism is beyond the scope of the current studies and methods.

Sequence Dependent DNA Cleavage using Supercoiled MCs. Historically, pox virus type IB topoisomerases have been useful in elucidating mechanistic aspects of topoisomerase reactions because of their specificity for cleavage at 5'-C/TCCTT-3' pentapyrimidine sequences[56,125]. The structural basis for their specificity has in part been suggested from the observed structural transition that occurs between the noncovalent and covalent enzyme-DNA complexes[67]. In this transition, α-helix 5 docks in the major groove upstream of the cleavage site, forming direct interactions with the DNA bases of the pentapyrimidine sequence. Accordingly, DNA cleavage studies using short DNA duplexes containing sequences that diverge from the consensus sequence show markedly reduced rates in the range 10 to 5000-fold for single base changes within the sequence[56,92]. To construct MC^{ns} from the specific substrate MC^{sp}, two base changes

were made (CCCTT→CGATT). These changes would be expected to decrease the rate of cleavage by ~10^5-fold if the known effects of the corresponding single base changes were energetically additive[92]. MC^{ns} also contains four other tetrapyrimidine sequences (also present in MC^{sp}) that should be cleaved at least 10^4-fold slower based on the sequence dependence of site cleavage with small duplexes. With these considerations, we anticipated that MC^{ns} would be at least 10^4-fold less reactive than MC^{sp}.

We were surprised to find that single-turnover cleavage of MC^{ns} occurred with a second-order rate only $1/30^{th}$ that of MC^{sp} (Figure 2.14A). In part, the reduced specificity with supercoiled MCs can be attributed to different rate-limiting steps for cleavage of MC^{sp} and MC^{ns}. For MC^{sp}, intramolecular transfer of the vTopo C clamp to the cleavage site is fully rate-limiting, while for MC^{ns} the slow step is most certainly cleavage. However, other factors could also contribute to the apparent reduction in sequence specificity for supercoiled DNA. Most notably, the dense concentration of nonspecific cleavage sites allows multiple vTopo molecules to act nonspecifically on the same substrate. It is also possible that a subtle structural effect of DNA supercoiling could enhance nonspecific cleavage relative to sequence specific cleavage.

Superhelical Density (Torque) and the Mechanism of Supercoil Unwinding. Single molecule DNA extension measurements have become the premiere method to investigate supercoil unwinding by type 1B topoisomerases[4,126]. Despite the unique insights provided by these approaches, there are merits to exploring such questions with ensemble methods using defined substrates such as employed here. First, the large (~25 kb) DNA substrates used in the single molecule methods contain ~30 sequences that are permutations of the vTopo cleavage recognition sequence, each of which has a unique

cleavage and ligation rate that can affect the observed unwinding originating from that site[54]. A similar situation applies to ensemble measurements with random plasmid sequences, but unlike single molecule methods, the ensemble average is not sensitive to rare relaxation events that deviate substantially from the ensemble mean. Second, since the single molecule measurements are made under applied force it is more difficult to study negatively supercoiled DNA because the DNA tends to denature. Thus, the most comprehensive single molecule measurements have been performed using positively supercoiled DNA with extrapolations to zero force to mimic the natural condition of supercoiled DNA in solution[54]. In contrast, the present ensemble measurements, and those previously made with pUC19, use negatively supercoiled minicircles, which could behave differently. Given these considerations we think it is unfounded to expect quantitative agreement between these experimental approaches. Nevertheless, both ensemble and single-molecule methods have converged on a processive mechanism for supercoil removal that involves removal of ~5 to 19 supercoils during the lifetime of the covalent complex[53,54,64].

The most informative new parameters derived from our current supercoil relaxation experiments with MC^{sp2} (1752 bp, 11.2 negative supercoils) are the partitioning ratios $k_{s \to p}/k_{s \to I1,2}$ and $k_{I1,2 \to p}/k_{lig}$ (Table 2). Taken together, the values $k_{s \to p}/k_{s \to I1} = 3.8$ and $k_{s \to p}/k_{s \to I2} = 2.1$ indicate that once cleavage occurs there is a net 0.5 probability that a substrate topoisomer of MC^{sp2} will unwind all 11 negative supercoils without forming any intermediate. It is noteworthy that our ability to observe intermediates is limited to two pools with low average superhelical densities. This suggests that the increased superhelical torque present in more highly supercoiled

topoisomer intermediates prevents their efficient trapping by strand ligation. Although the DNA rotation rate is driven by superhelical torque, which is expected to result in a decrease in the unwinding rate over the course of relaxation, this effect would not be directly observable in ensemble measurements because rotation is always more rapid than the rate of covalent complex formation and ligation. In contrast, single molecule experiments can directly detect unwinding by measuring the time dependent increase in DNA extension that results from supercoil relaxation[54]. Nevertheless, ensemble measurements can provide an estimate of the *average* duplex unwinding rate (in rotations s^{-1}) using the ligation rate constant as a clock. The kinetic basis for this estimate is that intermediate pools cannot be formed any faster than $k_{lig} = 4$ s^{-1} (i.e. $k_{lig} \geq k_{s \rightarrow I1,2}$). Using this upper limit for $k_{s \rightarrow I1}$, and the larger product partitioning ratio $k_{s \rightarrow p}/k_{s \rightarrow I1} = 3.8$, an upper limit for $k_{s \rightarrow p} \leq 16$ s^{-1} is obtained. Since 11 negative supercoils were removed in this time, the average unwinding rate is $k_{uw} \leq (11$ rotations$)(16$ $s^{-1}) \leq 180$ rotations s^{-1}.

In contrast to the large unwinding rate for highly supercoiled substrate topoisomers, the low values of $k_{I \rightarrow p}/k_{lig}$ in the range 0.003 to 0.0085 for pool I1 and I2 topoisomers indicate that cleavage and religation occur ~100-350 times for every unwinding event when torque is small. This kinetic regime amounts to rapid equilibrium cleavage/ligation followed by slow unwinding. To our knowledge, this is the first report of slow topoisomer unwinding in a regime of low superhelical torque and indicates that DNA domains with low superhelical density may persist longer in the presence of topoisomerases.

Controlled Rotation Mechanism. vTopo is known to make interactions with the rotating

DNA segment downstream of the cleavage site and such interactions have been previously implicated in supercoil unwinding[58,67]. Crystal structures show that residue K271 sits within helix 10 of vTopo and could contribute to positioning of the DNA segment downstream of the cleavage site to facilitate religation[59]. We anticipated that reversing the charge on this amino acid might decrease the probability for religation, resulting in an increased ratio $k_{s \to p}/k_{s \to i}$ ratio. Indeed, we found that K271E increased this ratio 2 and 7-fold for pool I1 and I2 as compared to the wild-type enzyme (Fig. 2.16C). Even though duplex rotation is rapid with wild-type vTopo, the results with the K271E enzyme indicate that the enzyme does form interactions with the DNA during relaxation that serve to reduce the number of supercoils that are unwound per cleavage event.

Mechanistic Utility of DNA Minicircles. The use of DNA minicircles has increased in recent years as more convenient synthesis and purification schemes have become available[97,98]. The majority of these uses have been in the area of gene therapy or for observing the local and long-range dynamics of short circularized DNA[95,96,127]. In contrast, there has been limited use of minicircles as substrates for enzymes that interact with specific DNA sites[69]. In this work, we showed how minicircle technology in combination with the capability to generate specific DNA sequences by gene synthesis allowed the creation of engineered supercoiled DNA substrates for investigation of specific mechanistic questions. These engineered MC's have additional features that will allow exploration of other interesting aspects of topoisomerase action on supercoiled substrates. These features include (i) the introduction of specific zinc finger protein binding sites distal to the vTopo site to explore the effects of frictional drag of bound

proteins on supercoil unwinding, and (ii) the opportunity to introduce chemically modified oligonucleotide sequences between engineered Nb. BbvC1 nicking sites that flank the vTopo cleavage site[128]. These modified sequences could include phosphorothioate or methylphosphonate backbone substitutions, or unnatural base substitutions at any one or multiple sites. Such substrates will expand the structure-function studies that are possible with topoisomerase enzymes.

Tables

Table 2.1 Superhelical densities, binding constants, and single-turnover kinetic constants for relaxation of MCs by WT vTopo.

	Number of Supercoils[a]	Superhelical Density[b]	k_{lim}' $(M^{-1}s^{-1})$	K_D[c] (nM)
MC^{sp}	-2.7 ± 1.1	-0.062	1.7×10^6	ND[d]
MC^{sp*}	-5.4 ± 1.7	-0.125	ND	ND
i^{-1}	-1[e]	-0.023	ND	ND
MC^{sp2}	-11.2 ± 1.4	-0.066	ND	ND
Pool I1	-7 ± 1[e]	-0.042	ND	ND
Pool I2	-4 ± 1[e]	-0.024	ND	ND
MC^{ns}	-2.7 ± 1.1	-0.062	5.9×10^4	0.38
MC^{ns*}	-5.4 ± 1.7	-0.125	ND	0.54
MC^{nsL}	0	0	ND	0.70

[a]Determined by band counting using chloroquine gel electrophoresis (Figs. 2.5 and 2.6). Reported as the mean and SD of a Gaussian fit. [b]Determined using eq 1. [c]Determined using eq 3. The units are nM of minicircle. [d]ND; not determined. [e]These values were calculated using the most prevalent topoisomer in the intermediate pool, which was then used to calculate the average superhelical density of the pool.

Table 2.2 Kinetic parameters for supercoil unwinding of MCs by WT and K271E vTopo.

	$k_{\lim}$ (s^{-1})	$k_{s\to p}/k_{s\to i}$	$k_{i\to p}/k_{\mathrm{lig}}{}^{c}$
MC^{sp}	0.029 ± 0.0012	ND	0.0074 ± 0.0016
MC^{sp*}	0.014 ± 0.0006	1.2 ± 0.12	0.008 ± 0.00088
MC^{sp2}	0.019 ± 0.0004		
	(0.0023 ± .000074)[b]		
Pool I1		2.1 ± 0.22	0.0084 ± 0.0013
		(7.7 ± 1.5)[b]	(0.017 ± 0.0094)[b]
Pool I2		3.8 ± 0.26	0.0032 ± 0.00026
		(15.1 ± 5.1)[b]	(0.013 ± 0.017)[b]

[a]Determined using numerical simulations. [b]Fitted parameters for K271E are shown in parentheses. [c]k_{lig} was set at 4 s^{-1} and 0.17 s^{-1} for the WT and K271E vTopo (see main text for justification).

Figures

GGGCGAATTGGGCCCGACGTCGCATGCTCCTCTAGA*CTCGAG*GAATTCCGTCTGCGAACGCCAGCAAGACGTAGCCCAGCGCGTCG
GCCGCCATGCCGGCGATAATGGCCTGCTTCTCGCCGAAACGTTTGGTGGCGGGACCAGTGACGAAGGCTTGAGCGAGGGCGTGCAA
GATTCCGAATACCGCAAGCGACAGGCCGATCATCGTCGCGCTCCAGCGAAAGCGGTCCTCGCCGAAAATGACCCAGAGCGCTGCCG
GCACCTGTCCTACGAGTTGCATGATAAAGAAGACAGTCATAAGTGCGGCGACGATAGTCATGCCCCGCGCCCACCGGAAGGAGCTG
ACTGGGTTGAAGGCTCTCAAGGGCATCGGGAAACTGAAAATGTGTTCACAGGTTGCTCCGGGCTATGAAATAGAAAAATGAATCCG
TTGAAGCCTGCTTTTTTATACTAACTTGAGCGCTGCAGTAAGCTTTACCTGAGCATGCGAATGCCAGCGTCAGACATCACATGCAG
ATACTCACCTGATGACTGAACGGATCGCCTCAGCGACCCTTATTCGGGTCGACGCTACCTCAGCAGCGATGCTAATGATGTCGATA
GTTACTAACGGGTCATTGTTCGATTAACTGCCGCAGCAACATCAGGCACCAGTAGCGTGGGCGTAAACAGTAGTGTTACCAGGATG
GCGAGCTTAGCAGTCGGTAAACCTGTCGTGCCAGCTGCATTAATGAATCAAGCTTGCTAGCATCTGTTACAGGTCACTAATACCAT
CTAAGTAGTTGATTCATAGTGACTGCATATGTTGTGTTTTACAGTATTATGTAGTCTGTTTATTATGCAAAATCTAATTTAATATA
TTGATATTTATATCATTTTACGTTGCTCGTTCAGCTTATTTATACTAAGTTGGCATTATAAAAAAGCATTGCTTATCAATTTGTTG
CAACGAACAGGTCACTATCAGTCAAAATAAAATCATTATTTGATTTCAATTTTGTCCCACTCCCTGCCTCTGTCATCACGATACTG
*TGATGCCATGG*TGTCCGACTTATGCCCGAGGATCCGGAGAGCTCCCAACGCGTTGGATGCATAGCTTGAGTATTCTATAGTGTCAC
CTAAATAGCTTGGCGTAATCATGGTCATAGCTGTTTCCTGTGTGAAATTGTTATCCGCTCACAATTCCACACAACATACGAGCCGG
AAGCATAAAGTGTAAAGCCTGGGGTGCCTAATGAGTGAGCTAACTCACATTAATTGCGTTGCGCTCACTGCCCGCTTTCCAGTCGG
GAAACCTGTCGTGCCAGCTGCATTAATGAATCGGCCAACGCGCGGGGAGAGGCGGTTTGCGTATTGGGCGCTCTTCCGCTTCCTCG
CTCACTGACTCGCTGCGCTCGGTCGTTCGGCTGCGGCGAGCGGTATCAGCTCACTCAAAGGCGGTAATACGGTTATCCACAGAATC
AGGGGATAACGCAGGAAAGAACATGTGAGCAAAAGGCCAGCAAAAGGCCAGGAACCGTAAAAAGGCCGCGTTGCTGGCGTTTTTCC
ATAGGCTCCGCCCCCCTGACGAGCATCACAAAAATCGACGCTCAAGTCAGAGGTGGCGAAACCCGACAGGACTATAAAGATACCAG
GCGTTTCCCCCTGGAAGCTCCCTCGTGCGCTCTCCTGTTCCGACCCTGCCGCTTACCGGATACCTGTCCGCCTTTCTCCCTTCGGG
AAGCGTGGCGCTTTCTCATAGCTCACGCTGTAGGTATCTCAGTTCGGTGTAGGTCGTTCGCTCCAAGCTGGGCTGTGTGCACGAAC
CCCCCGTTCAGCCCGACCGCTGCGCCTTATCCGGTAACTATCGTCTTGAGTCCAACCCGGTAAGACACGACTTATCGCCACTGGCA
GCAGCCACTGGTAACAGGATTAGCAGAGCGAGGTATGTAGGCGGTGCTACAGAGTTCTTGAAGTGGTGGCCTAACTACGGCTACAC
TAGAAGGACAGTATTTGGTATCTGCGCTCTGCTGAAGCCAGTTACCTTCGGAAAAAGAGTTGGTAGCTCTTGATCCGGCAAACAAA
CCACCGCTGGTAGCGGTGGTTTTTTTGTTTGCAAGCAGCAGATTACGCGCAGAAAAAAAGGATCTCAAGAAGATCCTTTGATCTTT
TCTACGGGGTCTGACGCTCAGTGGAACGAAAACTCACGTTAAGGGATTTTGGTCATGAGATTATCAAAAAGGATCTTCACCTAGAT
CCTTTTAAATTAAAAATGAAGTTTTAAATCAATCTAAAGTATATATGAGTAAACTTGGTCTGACAGTTACCAATGCTTAATCAGTG
AGGCACCTATCTCAGCGATCTGTCTATTTCGTTCATCCATAGTTGCCTGACTCCCCGTCGTGTAGATAACTACGATACGGGAGGGC
TTACCATCTGGCCCCAGTGCTGCAATGATACCGCGAGACCCACGCTCACCGGCTCCAGATTTATCAGCAATAAACCAGCCAGCCGG
AAGGGCCGAGCGCAGAAGTGGTCCTGCAACTTTATCCGCCTCCATCCAGTCTATTAATTGTTGCCGGGAAGCTAGAGTAAGTAGTT
CGCCAGTTAATAGTTTGCGCAACGTTGTTGCCATTGCTACAGGCATCGTGGTGTCACGCTCGTCGTTTGGTATGGCTTCATTCAGC
TCCGGTTCCCAACGATCAAGGCGAGTTACATGATCCCCCATGTTGTGCAAAAAAGCGGTTAGCTCCTTCGGTCCTCCGATCGTTGT
CAGAAGTAAGTTGGCCGCAGTGTTATCACTCATGGTTATGGCAGCACTGCATAATTCTCTTACTGTCATGCCATCCGTAAGATGCT
TTTCTGTGACTGGTGAGTACTCAACCAAGTCATTCTGAGAATAGTGTATGCGGCGACCGAGTTGCTCTTGCCCGGCGTCAATACGG
GATAATACCGCGCCACATAGCAGAACTTTAAAAGTGCTCATCATTGGAAAACGTTCTTCGGGGCGAAAACTCTCAAGGATCTTACC
GCTGTTGAGATCCAGTTCGATGTAACCCACTCGTGCACCCAACTGATCTTCAGCATCTTTTACTTTCACCAGCGTTTCTGGGTGAG
CAAAAACAGGAAGGCAAAATGCCGCAAAAAAGGGAATAAGGGCGACACGGAAATGTTGAATACTCATACTCTTCCTTTTTCAATAT
TATTGAAGCATTTATCAGGGTTATTGTCTCATGAGCGGATACATATTTGAATGTATTTAGAAAAATAAACAAATAGGGGTTCCGCG
CACATTTCCCCGAAAAGTGCCACCTGTATGCGGTGTGAAATACCGCACAGATGCGTAAGGAGAAAATACCGCATCAGGCGAAATTG
TAAACGTTAATATTTTGTTAAAATTCGCGTTAAATATTTGTTAAATCAGCTCATTTTTTAACCAATAGGCCGAAATCGGCAAAATC
CCTTATAAATCAAAAGAATAGACCGAGATAGGGTTGAGTGTTGTTCCAGTTTGGAACAAGAGTCCACTATTAAAGAACGTGGACTC
CAACGTCAAAGGGCGAAAAACCGTCTATCAGGGCGATGGCCCACTACGTGAACCATCACCCAAATCAAGTTTTTTGCGGTCGAGGT
GCCGTAAAGCTCTAAATCGGAACCCTAAAGGGAGCCCCCGATTTAGAGCTTGACGGGGAAAGCCGGCGAACGTGGCGAGAAAGGAA
GGGAAGAAAGCGAAAGGAGCGGGCGCTAGGGCGCTGGCAAGTGTAGCGGTCACGCTGCGCGTAACCACCACACCCGCCGCGCTTAA
TGCGCCGCTACAGGGCGCGTCCATTCGCCATTCAGGCTGCGCAACTGTTGGGAAGGGCGATCGGTGCGGGCCTCTTCGCTATTACG
CCAGCTGGCGAAAGGGGGATGTGCTGCAAGGCGATTAAGTTGGGTAACGCCAGGGTTTTCCCAGTCACGACGTTGTAAAACGACGG
CCAGTGAATTGTAATACGACTCACTATA

Figure 2.1 pMC454 Sequence.
The sequence in italics was generated by gene synthesis (IDT) and the MC^{sp} sequence is in color. The attR sequence is in purple. The specific CCCTT site is in red. The two Nb.BbvCI nicking sites and the zinc finger motif are in green. The PstI and NheI restrictions sites are underlined in purple. The 206-mer primer sites are underlined in blue. The NcoI and XhoI restriction sites are highlighted in yellow.
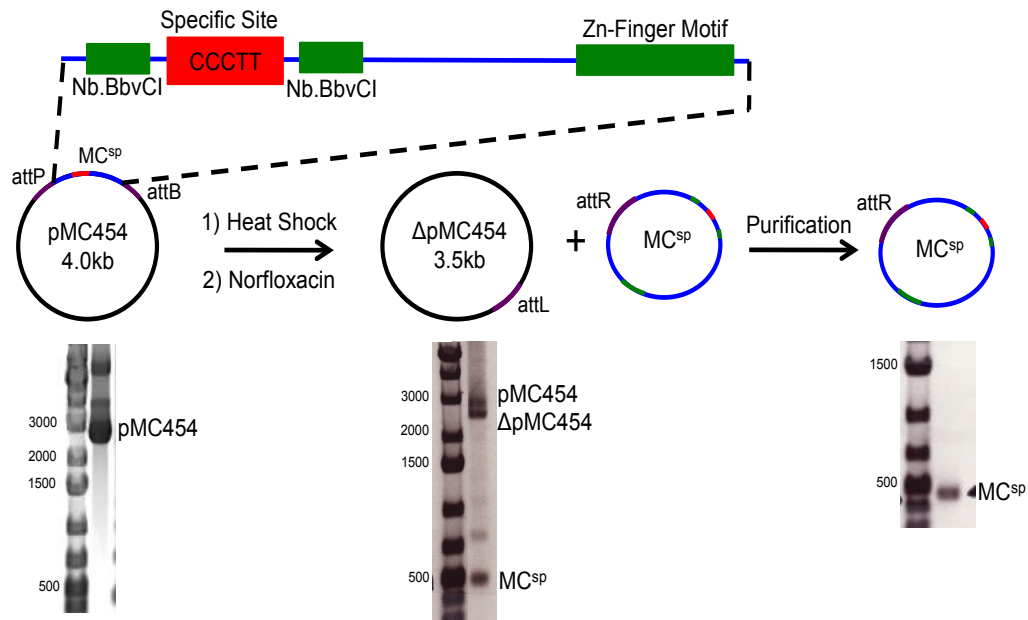
Figure 2.2 Minicircle (MC) preparation.
MCs containing a single vTopo cleavage site (CCCTT) were prepared by inserting an engineered DNA sequence between the attP and attB λ integration sites in plasmid pattD to give pMC454 (the attP and attB sites are in direct orientation). The engineered plasmid sequence was devoid of any other pentapyrimidine sequences that might serve as good cleavage sites, but also includes engineered nicking sites (Nb. BbvC1) and a zinc finger binding motif for future mechanistic explorations (see Discussion). For propagation and recovery of the MC plasmids, pMC454 was transformed into bacterial strain LZ54, which is lysogenic for λ bacteriophage and integrase expression was induced by heat shock. The addition of norfloxacin results in decatenation of the circular products of the disintegration reaction and MCs are purified by preparative agarose gel electrophoresis. The products of the integration reaction and purified MC^{sp} (454 bp) are shown. Gel electrophoresis was performed using a 1% agarose gel with visualization by EtBr staining.

GCTAGC<u>CTGCAG</u>TAACGTATACCTGAGCATGCGAATGCCAGCGTCAGACATCACATGC
AGATACTCACCTGATGACTGAACGGTACGCCAGAGCGAGACTTAGTCGGGTAAACG
CTACCAGAGCAGCGATGCTAATGCGATGTCGATAGTTACTAACGGGTCATTGTTCG
ATTAACTGCCGCAGCGATTAACATCAGGCACCAGTAGCATGACCATAAACAGTAGT
GTTACCAGGATGGCGAGCTTAGCAGTATGACGTAGCCTACGGTAAACCTGTCGTGC
CAGCTGCATTAATGAATCAACGTTTAACTTATACCTGAGCATGCCAATGCCAGCGT
CAGACATCACATGCATAGACTCACCTGATGACTCGAATAGGCGTCGGCCGCCATGC
CGCGATAATGGCCTGCTACTGCCGAACGTTGGTGGCTGACCAGTGACGAAGGCTTG
AGCGAGGGCGTGCAAGATTACCGAATACCGCAAGCGACAGGCCGAACATCGTCGCA
ACCAGCGAGTTCCGTCTGCGAACGCCAGCAAGACGTAGCCCAGCGTCGGCCATGTC
GCGAACACCGGAAGGAGCTGACTGTTGAAGGCGAACAAGGGCATCGGACTGAATGT
GTTCACAGGTTGCTCCAGGCTATGATAGAAT*GCTAGC*<u>CTGCAG</u>

Figure 2.3 Sequence of 661 bp oligonucleotide for constriction of pMC1103 and pMC1752.
PstI restriction sites are in italics and NheI restriction sites are underlined.

vTopo	-	+	+	+	+	+
[EtBr] (µg/mL)	-	-	0.25	0.5	1.0	1.5

ΔLk

0

-1

-2
-3

-4

-5
-6

100 nm
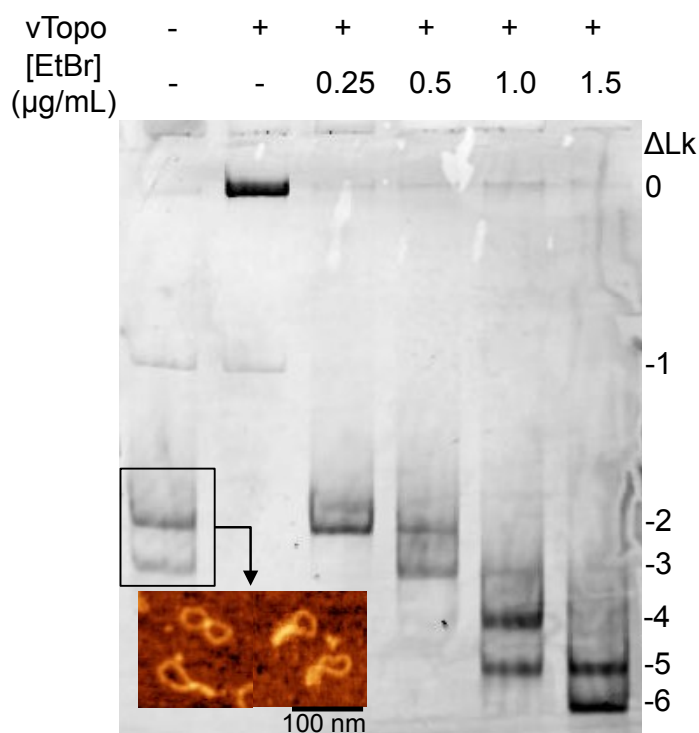
Figure 2.4 Minicircle supercoiling using ethidium bromide intercalation.
Following purification from bacterial cells, MC^{sp} has a superhelical density of -0.062. The insert shows an atomic force microscopy image of MC^{sp}. The images show the expected topological features of a supercoiled minicircle with superhelical density ~ -0.06. AFM was performed by deposition of MCs onto APS functionalized mica in air as described[129]. Lane 2 shows that reaction of MC^{sp} with vTopo collapses all supercoils into a single relaxed band with lower mobility. Increasing numbers of negative supercoils were introduced using *in vitro* reactions containing vTopo and increasing concentrations EtBr as indicated. After extraction of vTopo and EtBr intercalater, the DNA was isolated and subjected to polyacrylamide gel electrophoresis in the presence of $MgCl_2$ (shown). The negative linking numbers are indicated.
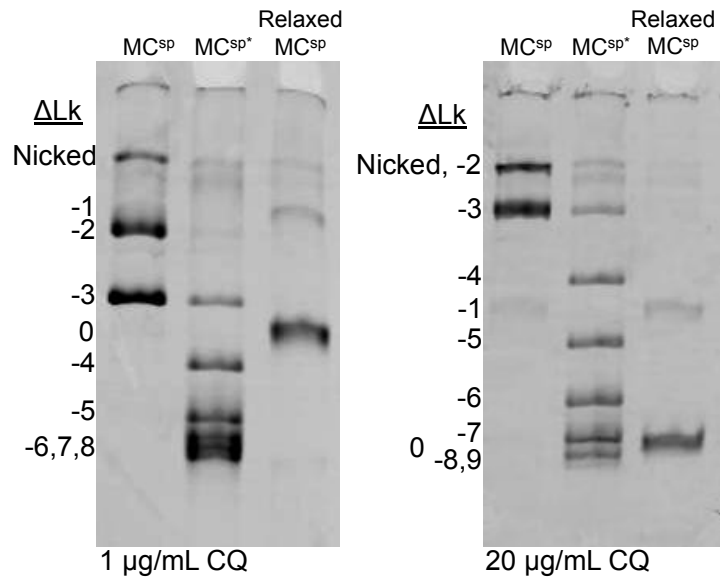
Figure 2.5 Determination of the average superhelical density of 454 bp minicircles MC^{sp} and MC^{sp*}.

Electrophoresis was performed using 5% native polyacrylamide gels run in 1X TBE and in the presence of the indicated amounts of chloroquine (CQ). Gels were run at 3 V/cm for 18 hours at room temperature. The average superhelical density was determined by fitting the bands to a Gaussian distribution in Prism and dividing by the number of helical turns in the DNA (turns = 454bp ÷ 10.5bp/turn) as described[102]. (See Table 1)
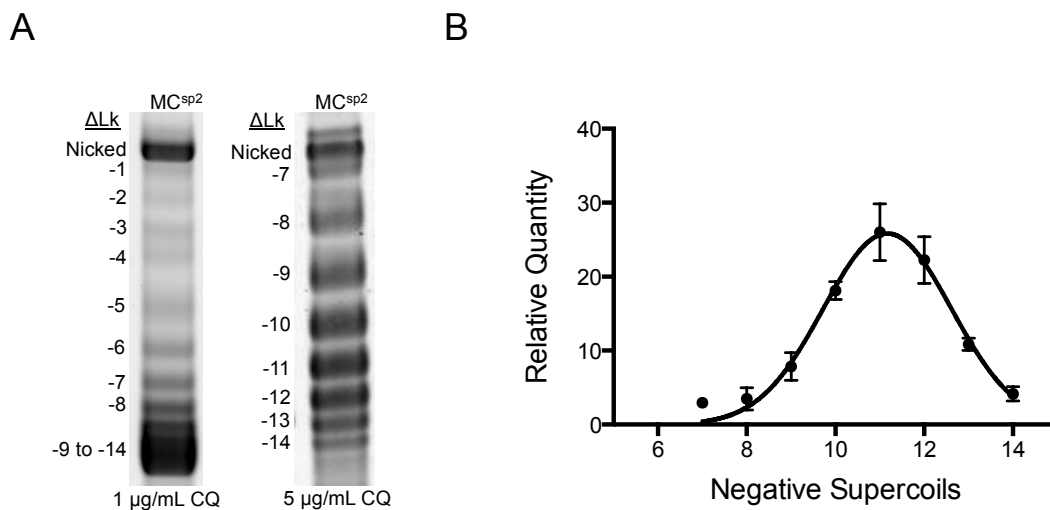
Figure 2.6 Determination of the average superhelical density of 1,752 bp MC^{sp2}.
(A) Electrophoresis was performed using 2% agarose gels run in presence of CQ and TAE Buffer. Gels were run at 4 V/cm for 17 hours at 4°C. (B) The average superhelical density was determined as described in the legend of Figure S1.
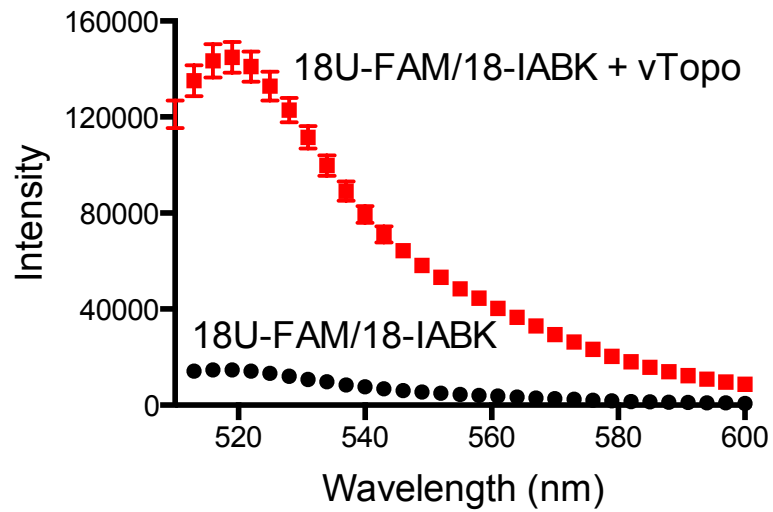
Figure 2.7 Fluorescence Emission Spectra.
Background corrected fluorescence emission spectra of 50 nM 18U-FAM/18-IABK before (black circles) and after (red squares) addition of 1 μM vTopo. A 10-fold fluorescence increase resulted from the complete cleavage of the substrate DNA by vTopo.
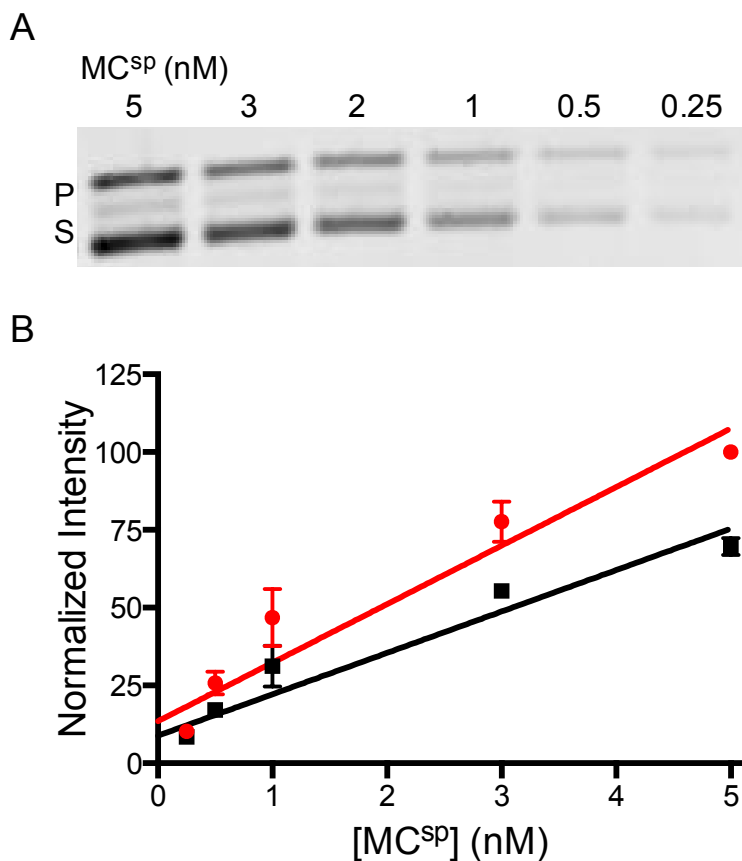
Figure 2.8. Differences in ethidium bromide (EtBr) staining between relaxed (P) and supercoiled (S) MC^{sp}.

(A) Equal concentrations (0.25 to 5 nM) of supercoiled and relaxed MC^{sp} were mixed and loaded onto a 2% agarose gel. Following electrophoresis, the gel was stained with EtBr, destained with distilled H$_2$O, and the bands were imaged. (B) The normalized fluorescence intensities (defined relative to the band with the greatest intensity) were determined and plotted against the known MC^{sp} concentration. The experiment was performed in duplicate and the slopes of the relaxed (black squares) and supercoiled (red circles) forms of MC^{sp} were determined. The ratio of the slopes (1.4) was taken as the correction factor in the experimental rate measurements. It is reasonably assumed that MC^{ns} behaves identically to MC^{sp} because it differs by only 2 bp.
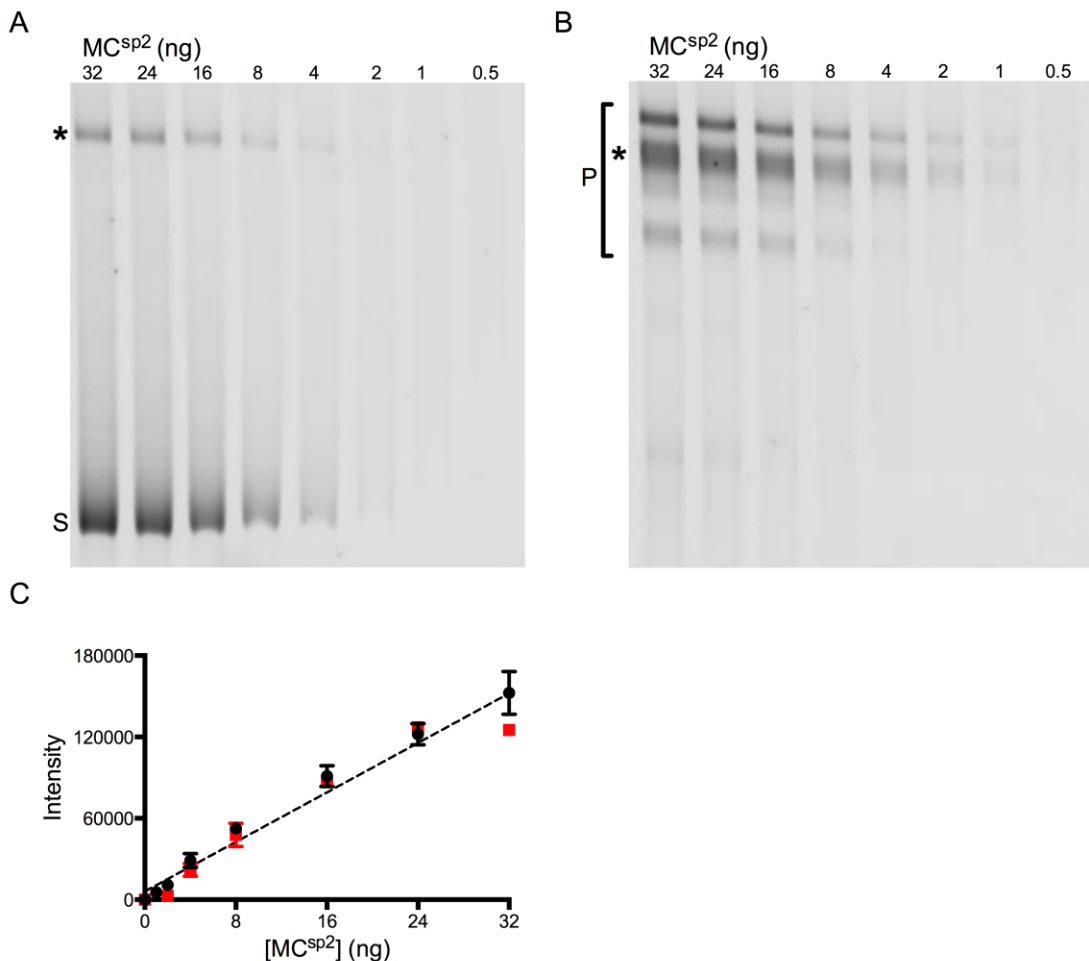
Figure 2.9 SYBR green staining in agarose gels is identical for the supercoiled (S) and relaxed (P) forms of MC^{sp2}.

The relaxed form of MC^{sp2} was generated by reacting supercoiled MC^{sp2} with vTopo under single turnover conditions of 10-fold excess vTopo as described in the Materials and Methods. The multiple product bands result from a thermal distribution of low superhelical density circular forms that persist after strand ligation. Equal concentrations of supercoiled (A) and relaxed (B) MC^{sp2} were loaded onto 3% agarose gels. Following electrophoresis, gels were stained with SYBR green and imaged as described. Gels were performed in duplicate. (C) The staining intensity was determined following subtraction of the intensity of the contaminating and overlapped nicked band (*) using the Gaussian fitting described in the main text. The substrate and products intensities were plotted against the known MC^{sp2} concentration. The relaxed (black circles) and supercoiled (red squares) forms of MC^{sp2} are fitted to the same line. In addition, this control establishes that MC^{sp2} stains linearly with SYBR Green up to 32 ng. Under our reaction conditions, no more than 24 ng of MC^{sp2} are loaded into any one lane on the gel.
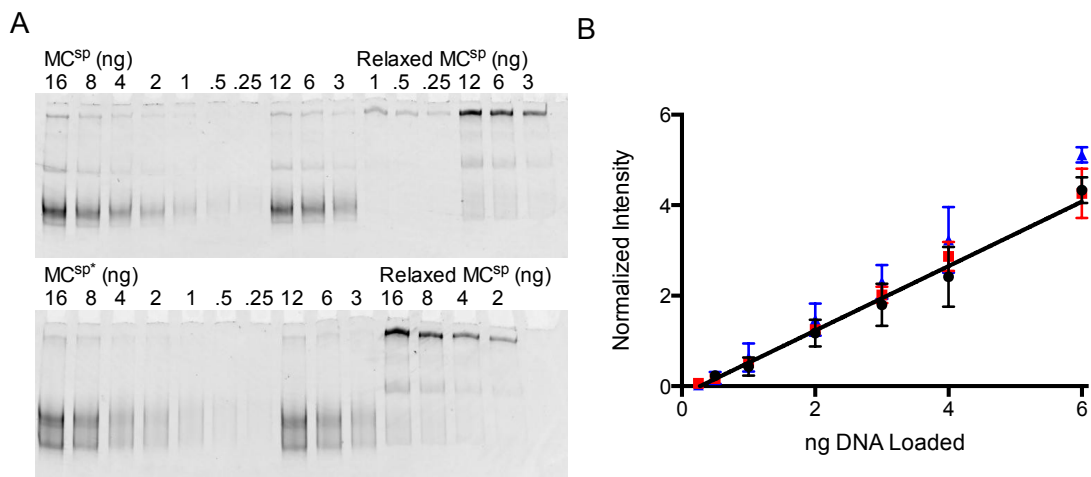
Figure 2.10 SYBR Green staining in polyacrylamide gels is identical for the supercoiled (S) and relaxed (P) forms of MC^{sp}.

The relaxed form of MC^{sp} was generated by reacting supercoiled MC^{sp} with vTopo under single turnover conditions of 10-fold excess vTopo as described in the Materials and Methods. (A) Equal concentrations of each topological form of MC^{sp} were loaded onto 6% acrylamide gels. Following electrophoresis, gels were stained with SYBR Green and imaged. (B) The staining intensity was determined using the Gaussian fitting method described in the main text and plotted against the known DNA concentration. The plots of MC^{sp} (black circles), MC^{sp*} (blue triangles), and relaxed MC^{sp} (red squares) were fitted to the same line. The fluorescence increase was linear with MC up to 6 ng. Under our reaction conditions, no more than 5 ng of MC^{sp} were loaded into any one lane on the gel. The experiment was performed in duplicate.

```
[task]

task = fit
data = progress

[mechanism]

ES --> ES* : klim
ES1 <--> ES1* : kcl klig
ES1* --> EP : ks1p
ES* --> EP : ksp

[constants]

klim = .02?
kcl = 0.3
klig = 4
ksp = 2?
Ks1p = .03?

[concentrations]

ES = 3.6
ES1 = 0.55
EP = 0

[progress]

directory    ./Breeana/data
extension    txt
file         MC454IntP | response EP = 1
file         MC454IntI | response ES1 = 1
file         MC454IntS | response ES = 1

[output]

directory    ./Breeana/output/MC454Int

[end]
```

Figure 2.11 Dynafit Input File for MC^{sp}.

```
[task]

task = fit
data = progress

[mechanism]

ES --> ES* : klim
ES* --> EI : ksi
EI <--> EI* : kcl klig
EI* --> EP : kip
ES* --> EP : ksp

[constants]

klim = .02?
kcl = 0.3
klig = 4
ksp = 10?
kip = .18?
ksi = 6?

[concentrations]

ES = 4.8
EI = 0
EP = 0

[progress]

directory    ./Breeana/data
extension    txt
file         MC454SCIntP | response EP = 1
file         MC454SCIntI | response EI = 1
file         MC454SCIntS | response ES = 1

[output]

directory    ./Breeana/output/MC454SCInt

[end]
```

Figure 2.12 Dynafit Input File for MC^{sp*}.

```
[task]

task = fit
data = progress

[mechanism]

ES --> ES* : klim
ES* --> EI1 : ksi1
EI1 <--> EI1* : kcl klig
EI1* --> EP : ki1p
ES* --> EI2 : ksi2
EI2 <--> EI2* : kcl klig
EI2* --> EP : ki2p
ES* --> EP : ksp

[constants]

klim = .017?
kcl = 0.3
klig = 4
ksp = 10?
ki1p = .05?
ki2p = .019?
ksi1 = 1?
ksi2 = .8?

[concentrations]

ES = 4
EI1 = 0
EI2 = 0
EP = 0

[progress]

directory    ./Breeana/data
extension    txt
file         MC1752P | response EP = 1
file         MC1752I123 | response EI1 = 1
file         MC1752I45 | response EI2 = 1
file         MC1752S | response ES = 1

[output]

directory    ./Breeana/output/MC1752IPool

-    ..
```

Figure 2.13 Dynafit Input File for MC^{sp2} with WT vTopo.

```
[task]

task = fit
data = progress

[mechanism]

ES --> ES* : klim
ES* --> EI1 : ksi1
EI1 <--> EI1* : kcl klig
EI1* --> EP : ki1p
ES* --> EI2 : ksi2
EI2 <--> EI2* : kcl klig
EI2* --> EP : ki2p
ES* --> EP : ksp

[constants]

klim = .002?
kcl = 0.0129
klig = .17
ksp = 10?
ki1p = 2?
ki2p = 2?
ksi1 = 1?
ksi2 = 1?

[concentrations]

ES = 4
EI1 = 0
EI2 = 0
EP = 0

[progress]

directory    ./Breeana/data
extension    txt
file         MC1752MP | response EP = 1
file         MC1752M123 | response EI1 = 1
file         MC1752M2 | response EI2 = 1
file         MC1752MS | response ES = 1

[output]

directory    ./Breeana/output/MC1752IMPool

-    ..
```

Figure 2.14 Dynafit Input File for MC^{sp2} with K271E vTopo.
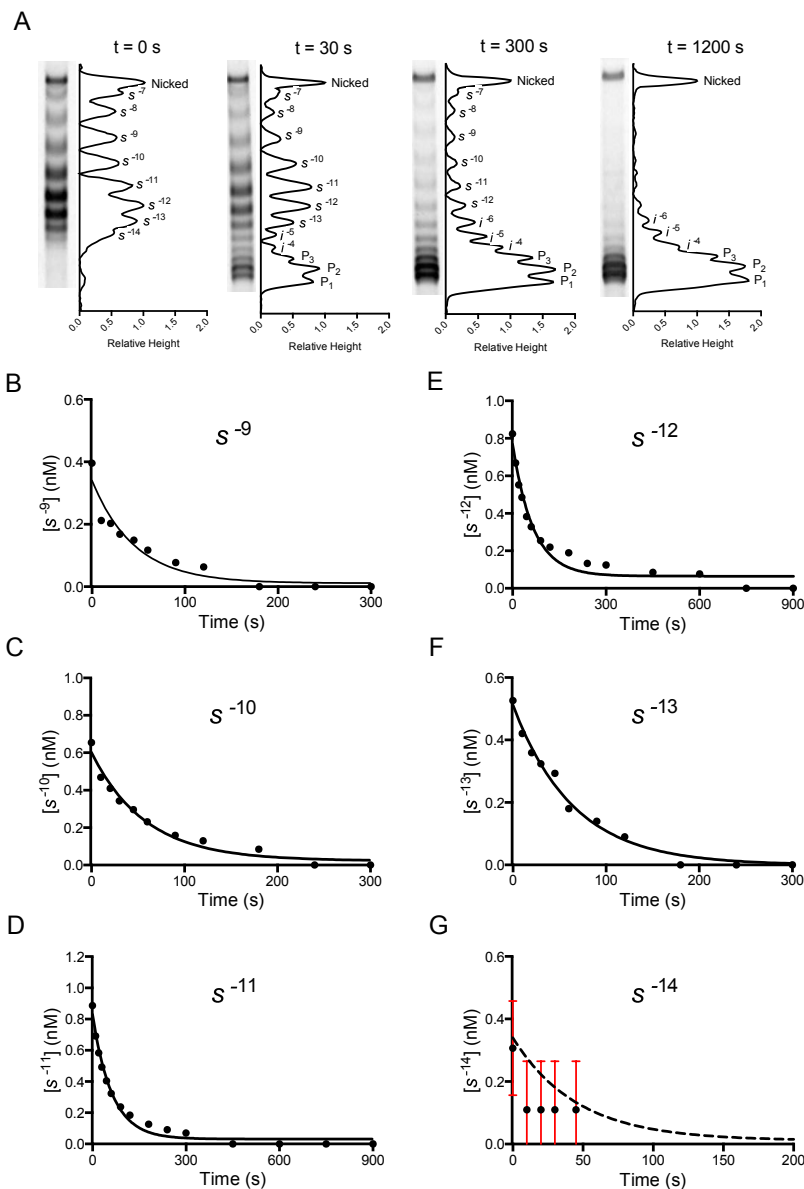
Figure 2.15 Resolved substrate ($s^{-9 \text{ to } -14}$) topoisomers of MC^{sp2} relax with the same rates.

(A) 5 nM MC^{sp2} was relaxed with 5 nM vTopo. The substrate topoisomers were resolved by electrophoresis using 2% agarose gels run in presence of 5 μg/mL CQ. The band intensities of the individual topoisomer bands s^{-9}-s^{-14} were quantified using the Gaussian shape fitting method in the Quantity One software and the integrated intensities were fitted to single exponential decays. (B-G) Individual decay time courses for s^{-9}-s^{-14}. The decay rate constants were identical for each substrate topoisomer between s^{-9} and s^{-13} ($k_{\lim} = 0.019 \pm 0.0004$ s^{-1}). The small amount of the minor topoisomer s^{-14} made the Gaussian curve fitting difficult. The error bars estimate the upper and lower limits of the s^{-14} band areas and the dashed curve is drawn using the $k_{\lim}$ value measured for the other substrate topoisomers. These results support the simplified model where s^{-9}-s^{-14} were treated as a substrate pool (S) rather than individual topoisomers.
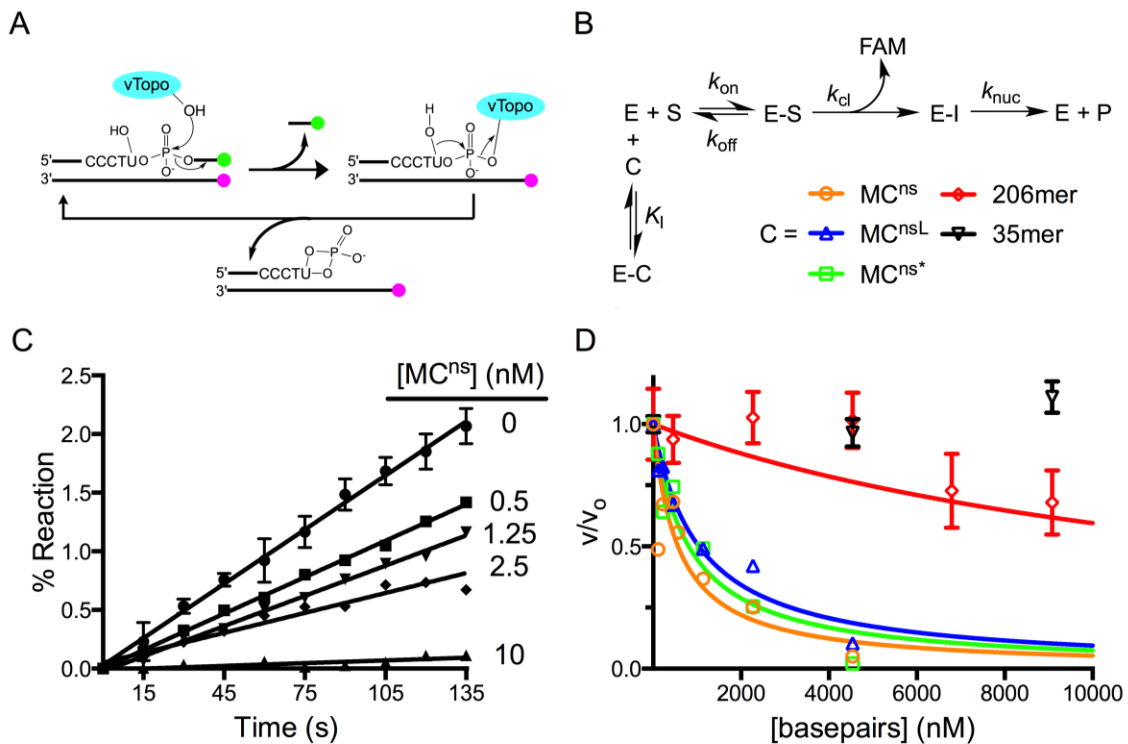
Figure 2.16 Competition assay to measure binding affinity of vTopo to various topological isoforms of MC^{ns} and nonspecific linear DNAs of varying length.
(A) Schematic of the continuous multiple turnover fluorescence assay for measuring vTopo catalyzed strand cleavage. The formation of a covalent complex between vTopo and the substrate releases a highly fluorescent 3′ FAM-labeled 7mer that is otherwise quenched in the duplex substrate by the IABK quench group on the opposite strand's 5′ end. The presence of the uracil ribonucleotide in the cleavage sequence (CCCTU) results in release of vTopo by nucleophilic attack by the 2′-OH group[105]. Thus, multiple steady-state turnovers are possible and initial linear rates can be accurately measured. (B) Competition binding mechanism. Since the K_m for the fluorescent substrate is known, the K_i for each competitive inhibitor (C) can be determined from the concentration dependence of the decrease in fractional velocity (v_i/v_o) using eq 3. (C) Steady-state initial rates as a function of [MC^{ns}]. Error bars have been removed for clarity but are of similar magnitude to those shown. The concentrations indicated are based on plasmid molecular weight. (D) Fractional velocity as a function of nucleic acid inhibitor concentration. To normalize for the different lengths of DNA used, the concentration is noted in molar base pairs. Most error bars have been omitted for clarity but are similar to those shown.

73
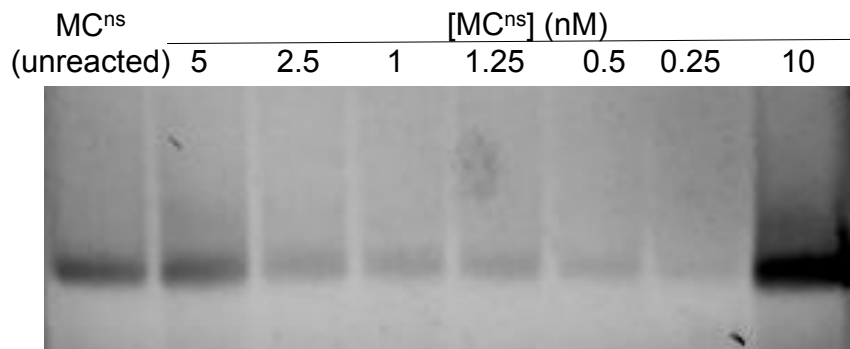
Figure 2.17 MC^{ns} isolated from competition binding assays remains supercoiled during the course of the experiment.
Following the 180 s competition binding experiment (see Materials and Methods), the entire reaction volume was removed from each cuvette and quenched with 150 µL of 2X Quench Buffer. Fifty-five microliters of the quenched reaction were then loaded onto a 2% agarose gel in 1X TAE and run for 45 min. at 100 V. The gel was stained with SYBR Green and imaged. The gel image shows that all concentrations of MC^{ns} used in the competition binding experiment migrate with the same mobility as the control supercoiled MC (leftmost lane). Thus, MC^{ns} was not relaxed by vTopo during the course of the binding reactions.
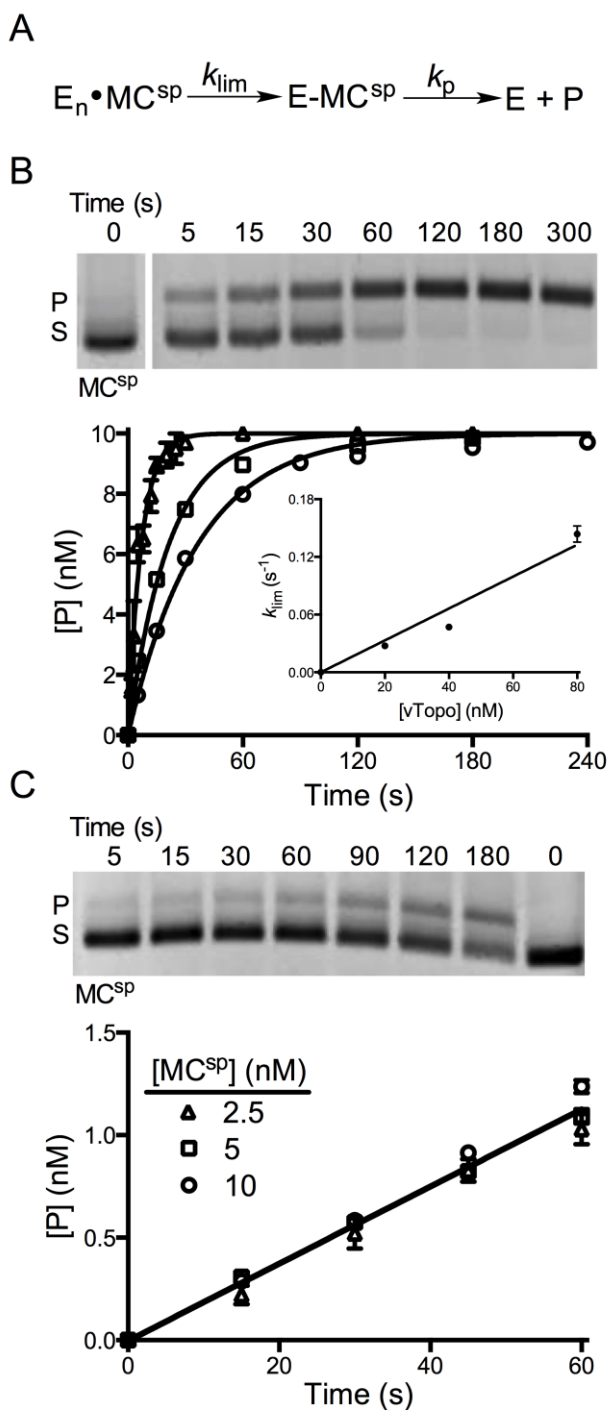
Figure 2.18 Cleavage activity of vTopo with MC^{sp}.

(A) Cleavage and supercoil unwinding reactions involve a binding step, an intramolecular search mechanism, and reversible strand cleavage (k_{lim}) prior to the formation of product through supercoil unwinding (k_p). (B) Single-turnover cleavage and supercoil unwinding. Supercoil unwinding of 10 nM MC^{sp} in the presence of 20 nM (circles), 40 nM (squares), or 80 nM (triangles) concentrations of vTopo. The gel image shows the time course for relaxation of MC^{sp} by 40 nM vTopo (S is the supercoiled substrate and P is the relaxed product). The data were fitted to a first-order rate equation for the appearance of product and confirmed using *Dynafit 3*. The values of k_{lim} were plotted against enzyme concentration and gave a linear response with respect to enzyme concentration over the accessible range (inset). Some error bars have been omitted for clarity, but are similar to those shown. (C) Steady-state turnover under initial rate conditions. The relaxation of 5 nM MC^{sp} in the presence of 1 nM vTopo is shown in the gel image. The rate was independent of DNA concentration in the range 2.5 to 10 nM, indicating that the enzyme is saturated with DNA and the maximal steady-state velocity is being measured.

A

Time (s)
60 120 180 300 420 540 720 900   0

P
S
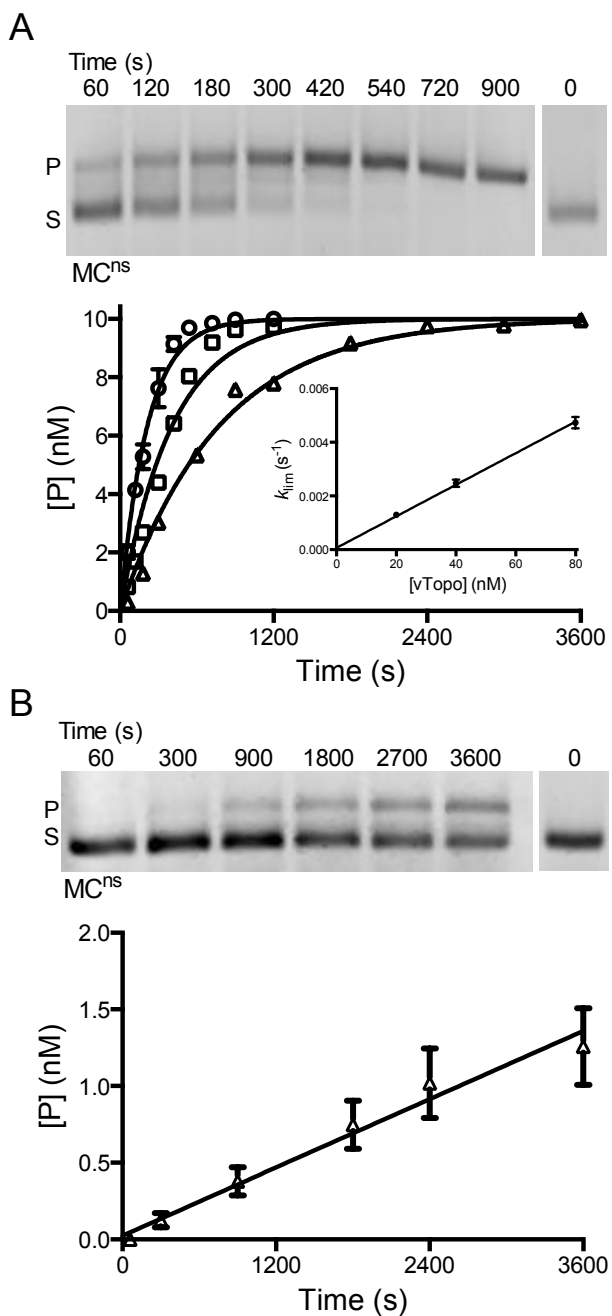
MC^{ns}

Figure 2.19 Activity of vTopo with MC^{ns}, a MC that does not contain a consensus cleavage site. (A) Single turnover cleavage and supercoil unwinding. The gel image shows the time course for relaxation of 10 nM MC^{ns} by 80 nM vTopo (S is the supercoiled substrate and P is the relaxed product). MC^{ns} was also reacted with 20 nM (triangles), 40 nM (squares) or 80 nM (circles) concentrations of vTopo. The data were fitted to a first-order rate equation. The values of k_{lim} were plotted against enzyme concentration and were linear with respect to enzyme concentration over the accessible range (inset). Some error bars have been omitted for clarity, but are similar to those shown. (B) Steady-state turnover under initial rate conditions. The relaxation of 2.5 nM MC^{sp} in the presence of 1 nM vTopo is shown in the gel image.

B

Time (s)
60   300   900 1800 2700 3600   0

P
S

MC^{ns}
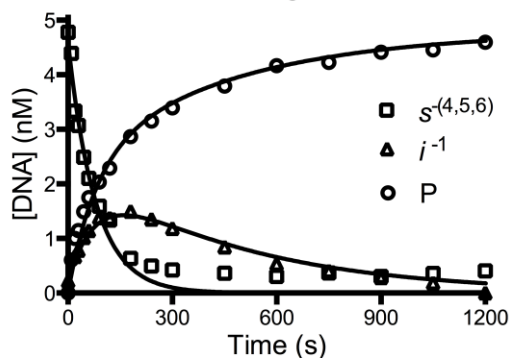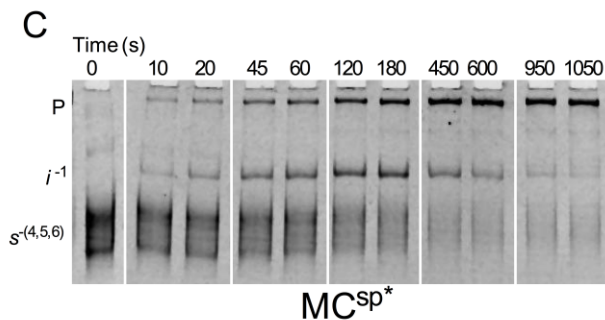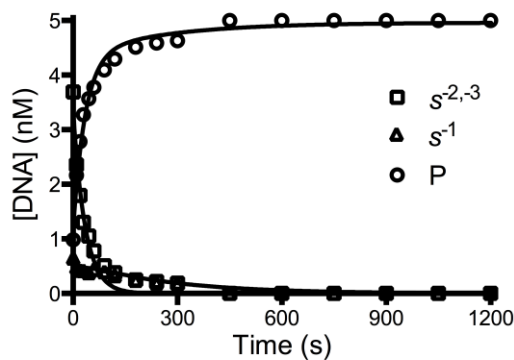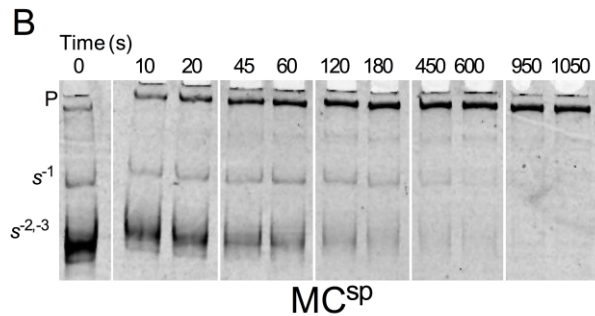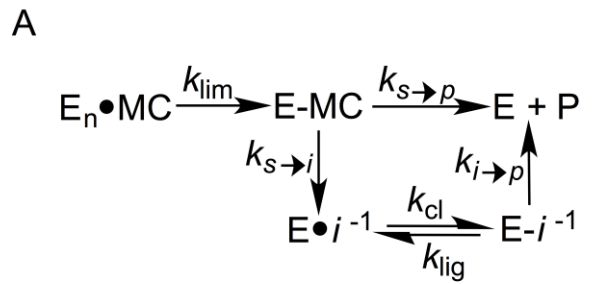
Figure 2.20 Mechanism of supercoil unwinding using MC^{sp} and MC^{sp*}.
(A) The use of small minicircles with the potential to form a limited number of topoisomer intermediates facilitates resolution and allows use of a simple kinetic model for the partitioning of the enzyme-minicircle covalent complex (E-MC) between complete unwinding to form product (P) and formation of intermediates (I). Intermediates result from kinetic competition between strand ligation ($k_{s \to i}$) and supercoil unwinding ($k_{s \to p}$). The competition between these processes determines the number of supercoils that are released for each rate limiting cleavage event. For brevity, only selected time points are shown. (B) Supercoil unwinding kinetics of MC^{sp} that contains 2 ± 1 negative supercoils. The reaction contained 5 nM MC^{sp} and 5 nM vTopo. (C) Supercoil unwinding kinetics of highly supercoiled MC^{sp*} that contains an average of 6 ± 2 negative supercoils. The reaction contained 5 nM MC^{sp*} and 5 nM vTopo. For both reactions, the time dependence of the substrate (S), product (P), and topoisomer intermediate (I) concentrations were fitted by numerical integration with least-squares optimization to the data using the program *Dynafit 3* and employing the model in panel A.
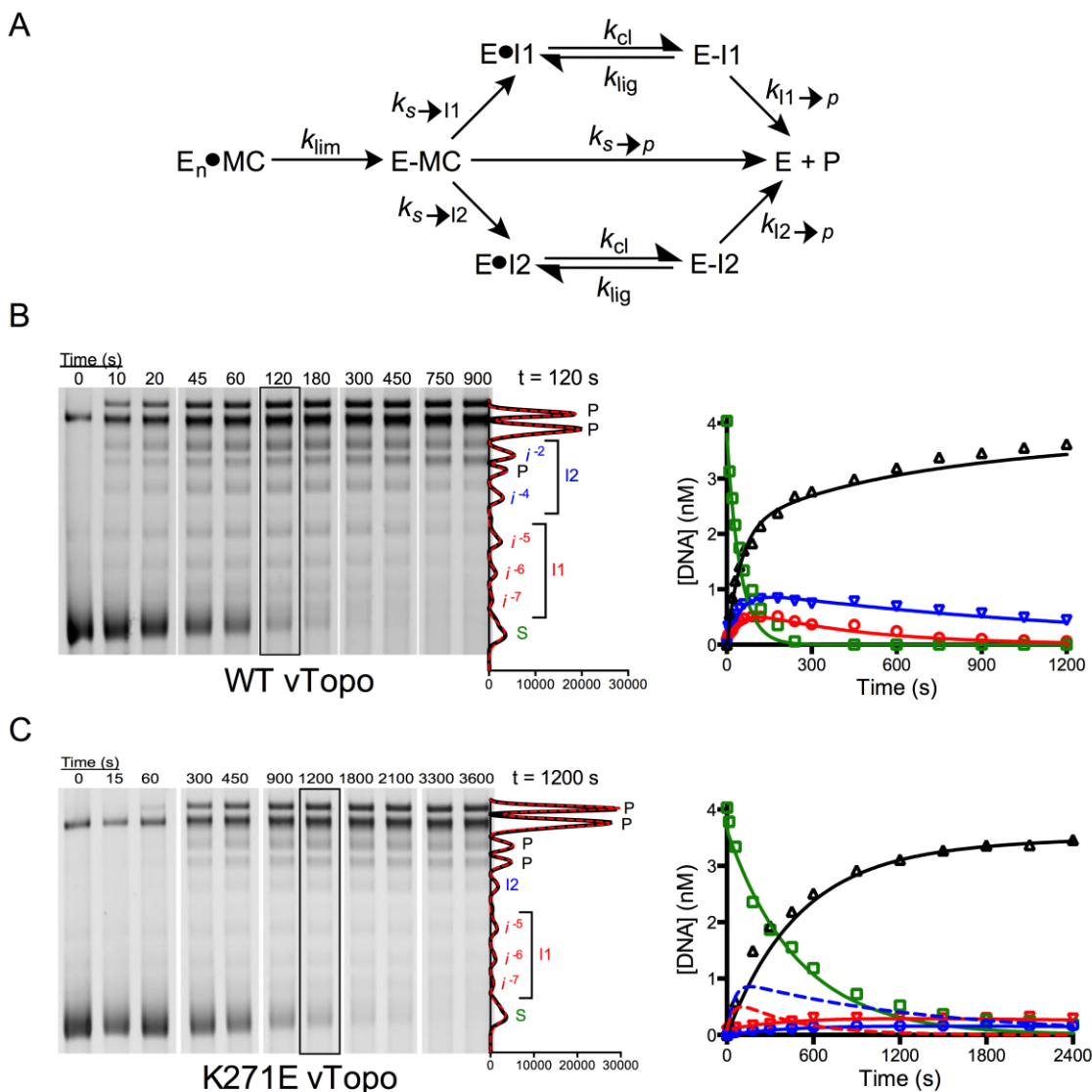
Figure 2.21 Processivity of supercoil unwinding by wild-type vTopo and the K271E mutant using the highly supercoiled MC^{sp2}.

For clarity, only selected time points are shown in the gel figures. (A) Kinetic Model for the disappearance of substrate into product and two intermediate pools (I1, I2), followed by reversible cleavage and unwinding of intermediate pools to product. (B) Time course for unwinding using 5 nM MC^{sp2} and 5 nM wild-type vTopo. Substrate (S), product (P), and intermediate bands (i^{-2} to i^{-7}) were resolved by gel electrophoresis, visualized by Sybr green staining, imaged and quantified using the Gaussian curve fitting routine in QuantityOne. A representative plot of the Gaussian fits for the time point at 120 s is shown on the right of the panel. The time courses for the appearance and disappearance of substrate (green), products (black) and intermediate pools (blue and red) were fitted by numerical integration and least-squares minimization to a stepwise supercoil unwinding model shown in and Panel A and Supplemental Materials. (C) Time course for unwinding using 5 nM MC^{sp2} and 5 nM K271E mutant. All steps in data acquisition and analysis are identical to those described in (A).

78

References

1.   Vologodskii, A. V., Levene, S. D., Klenin, K. V., Frank-Kamenetskii, M. & Cozzarelli, N. R. Conformational and thermodynamic properties of supercoiled DNA. *J Mol Biol* **227,** 1224–1243 (1992).

2.   R Dulbecco, M. V. Evidence for a Ring Structure of Polyoma Virus DNA. *Proc Natl Acad Sci USA* **50,** 236 (1963).

3.   Weil, R. & Vinograd, J. The Cyclic Helix and Cyclic Coil Form of Polyoma Viral DNA. *Proc Natl Acad Sci USA* **50,** 730–738 (1963).

4.   Koster, D. A., Crut, A., Shuman, S., Bjornsti, M.-A. & Dekker, N. H. Cellular strategies for regulating DNA supercoiling: a single-molecule perspective. *Cell* **142,** 519–530 (2010).

5.   Liu, L. F. & Wang, J. C. Supercoiling of the DNA template during transcription. *Proc Natl Acad Sci USA* **84,** 7024–7027 (1987).

6.   Postow, L., Crisona, N. J., Peter, B. J., Hardy, C. D. & Cozzarelli, N. R. Topological challenges to DNA replication: conformations at the fork. *Proc Natl Acad Sci USA* **98,** 8219–8226 (2001).

7.   Cozzarelli, N. R., Cost, G. J., Nöllmann, M., Viard, T. & Stray, J. E. Giant proteins that move DNA: bullies of the genomic playground. *Nat Rev Mol Cell Biol* **7,** 580–588 (2006).

8.   Neuman, K. C. Single-molecule measurements of DNA topology and topoisomerases. *J Biol Chem* **285,** 18967–18971 (2010).

9.   Wang, J. C. Cellular roles of DNA topoisomerases: a molecular perspective. *Nat Rev Mol Cell Biol* **3,** 430–440 (2002).

10. Carter, S. D. & Sjögren, C. The SMC complexes, DNA and chromosome topology: right or knot? *Crit Rev Biochem Mol Biol* **47,** 1–16 (2012).

11. Wang, J. C. & Lynch, A. S. Transcription and DNA supercoiling. *Curr Opin Genet Dev* **3,** 764–768 (1993).

12. Baxter, J. *et al.* Positive Supercoiling of Mitotic DNA Drives Decatenation by Topoisomerase II in Eukaryotes. *Science* **331,** 1328–1332 (2011).

13. Rampakakis, E., Gkogkas, C., Di Paola, D. & Zannis-Hadjopoulos, M. Replication initiation and DNA topology: The twisted life of the origin. *J. Cell. Biochem.* **110,** 35–43 (2010).

14. Watson, J. D. & Crick, F. H. Molecular structure of nucleic acids; a structure for deoxyribose nucleic acid. *Nature* **171,** 737–738 (1953).

15. Strick, T. R., Allemand, J. F., Bensimon, D. & Croquette, V. Behavior of Supercoiled DNA. *Biophys J* **74,** 2016–2028 (1998).

16. Eckdahl, T. Investigating DNA Supercoiling. *The American Biology Teacher* **61,** 214–216 (1999).

17. White, J. H. & Bauer, W. R. Calculation of the twist and the writhe for representative models of DNA. *J Mol Biol* **189,** 329–341 (1986).

18. Boles, T. C., White, J. H. & Cozzarelli, N. R. Structure of plectonemically supercoiled DNA. *J Mol Biol* **213,** 931–951 (1990).

19. Fogg, J. M. *et al.* Bullied no more: when and how DNA shoves proteins around. *Q Rev Biophys* **45,** 257–299 (2012).

20. Liu, L. F. & Wang, J. C. Supercoiling of the DNA template during transcription. (1987).

21.   Dunaway, M. & Ostrander, E. A. Local domains of supercoiling activate a eukaryotic promoter in vivo. *Nature* **361,** 746–748 (1993).

22.   Baranello, L., Levens, D., Gupta, A. & Kouzine, F. The importance of being supercoiled: How DNA mechanics regulate dynamic processes. *Biochim Biophys Acta* (2012). doi:10.1016/j.bbagrm.2011.12.007

23.   Rohs, R. *et al.* Origins of specificity in protein-DNA recognition. *Annual review of biochemistry* **79,** 233–269 (2010).

24.   Cavalli, G. & Misteli, T. Functional implications of genome topology. *Nat Struct Mol Biol* **20,** 290–299 (2013).

25.   Hsieh, T.-S. & Wang, J. C. Thermodynamic properties of superhelical DNAs. *Biochemistry* **14,** 527–535 (1975).

26.   Vinograd, J., Lebowitz, J., Radloff, R., Watson, R. & Laipis, P. The twisted circular form of polyoma viral DNA. *Proc Natl Acad Sci USA* **53,** 1104–1111 (1965).

27.   Wasserman, S. A. & Cozzarelli, N. R. Biochemical topology: applications to DNA recombination and replication. *Science* **232,** 951–960 (1986).

28.   Wu, H., Shyy, S., Wang, J. & Liu, L. Transcription generates positively and negatively supercoiled domains in the template. *Cell* (1988).

29.   Tsao, Y.-P., Wu, H.-Y. & Liu, L. F. Transcription-driven supercoiling of DNA: Direct biochemical evidence from in vitro studies. *Cell* **56,** 111–118 (1989).

30.   Wang, Z. & Dröge, P. Long-range effects in a supercoiled DNA domain generated by transcription in vitro. *J Mol Biol* **271,** 499–510 (1997).

31.   Levinthal, C. & Crane, H. R. ON THE UNWINDING OF DNA. *Proc Natl*

Acad Sci USA **42,** 436–438 (1956).

32.   van Loenhout, M. T. J., de Grunt, M. V. & Dekker, C. Dynamics of DNA
        Supercoils. *Science* (2012). doi:10.1126/science.1225810

33.   Leng, F. & McMacken, R. Potent stimulation of transcription-coupled DNA
        supercoiling by sequence-specific DNA-binding proteins. *Proc Natl Acad Sci
        USA* **99,** 9139–9144 (2002).

34.   Leng, F., Chen, B. & Dunlap, D. D. Dividing a supercoiled DNA molecule into
        two independent topological domains. *Proc Natl Acad Sci USA* (2011).
        doi:10.1073/pnas.1109854108

35.   Champoux, J. J. DNA topoisomerases: structure, function, and mechanism.
        Annual review of biochemistry **70,** 369–413 (2001).

36.   Redinbo, M. R., Champoux, J. J. & Hol, W. G. Structural insights into the
        function of type IB topoisomerases. *Curr Opin Struct Biol* **9,** 29–36 (1999).

37.   Zechiedrich, E. L. *et al.* Roles of topoisomerases in maintaining steady-state
        DNA supercoiling in Escherichia coli. *J Biol Chem* **275,** 8103–8113 (2000).

38.   Wang, J. C. DNA Topoisomerases. *Annual review of biochemistry* **65,** 635–692
        (1996).

39.   Wang, J. C. Interaction between DNA and an Escherichia coli protein omega. *J
        Mol Biol* **55,** 523–533 (1971).

40.   Chen, S. H., Chan, N.-L. & Hsieh, T.-S. New mechanistic and functional
        insights into DNA topoisomerases. *Annual review of biochemistry* **82,** 139–170
        (2013).

41.   Champoux, J. J. DNA topoisomerase I-mediated nicking of circular duplex

DNA. *Methods Mol Biol* **95,** 81–87 (2001).

42.   Liu, L. F., Liu, C. C. & Alberts, B. M. Type II DNA topoisomerases: enzymes that can unknot a topologically knotted DNA molecule via a reversible double-strand break. *Cell* **19,** 697–707 (1980).

43.   Forterre, P., Gribaldo, S., Gadelle, D. & Serre, M.-C. Origin and evolution of DNA topoisomerases. *Biochimie* **89,** 427–446 (2007).

44.   Schoeffler, A. J. & Berger, J. M. DNA topoisomerases: harnessing and constraining energy to govern chromosome topology. *Q Rev Biophys* **41,** 41–101 (2008).

45.   Yang, W. Topoisomerases and site-specific recombinases: similarities in structure and mechanism. *Crit Rev Biochem Mol Biol* **45,** 520–534 (2010).

46.   Strick, T. R., Croquette, V. & Bensimon, D. Single-molecule analysis of DNA uncoiling by a type II topoisomerase. *Nature* **404,** 901–904 (2000).

47.   Wang, J. C. Moving one DNA double helix through another by a type II DNA topoisomerase: the story of a simple molecular machine. *Q Rev Biophys* **31,** 107–144 (1998).

48.   Bugreev, D. V. & Nevinsky, G. A. Structure and mechanism of action of type IA DNA topoisomerases. *Biochemistry Moscow* **74,** 1467–1481 (2010).

49.   Dekker, N. H. *et al.* The mechanism of type IA topoisomerases. *Proc Natl Acad Sci USA* **99,** 12126–12131 (2002).

50.   Fernandez-Beros, M. & Tse-Dinh, Y. Vaccinia virus DNA topoisomerase I preferentially removes positive supercoils from DNA. *FEBS Lett* (1996).

51.   Shuman, S. & Prescott, J. Specific DNA cleavage and binding by vaccinia virus

DNA topoisomerase I. *J Biol Chem* **265,** 17826–17836 (1990).

52.   Champoux, J. DNA Topoisomerases: Structure, Function, and Mechanism. *Annual review of biochemistry* (2001).

53.   Stivers, J. T., Harris, T. K. & Mildvan, A. S. VacciniaDNA Topoisomerase I: Evidence Supporting a Free Rotation Mechanism for DNA Supercoil Relaxation †. *Biochemistry* **36,** 5212–5222 (1997).

54.   Koster, D. A., Croquette, V., Dekker, C., Shuman, S. & Dekker, N. H. Friction and torque govern the relaxation of DNA supercoils by eukaryotic topoisomerase IB. *Nature* **434,** 671–674 (2005).

55.   Sekiguchi, J. & Shuman, S. Vaccinia topoisomerase binds circumferentially to DNA. *J Biol Chem* **269,** 31731–31734 (1994).

56.   Shuman, S. Vaccinia virus DNA topoisomerase: a model eukaryotic type IB enzyme. *Biochim Biophys Acta* **1400,** 321–337 (1998).

57.   Redinbo, M. R., Stewart, L., Kuhn, P., Champoux, J. J. & Hol, W. G. Crystal structures of human topoisomerase I in covalent and noncovalent complexes with DNA. *Science* **279,** 1504–1513 (1998).

58.   Jun, H. & Stivers, J. T. Diverse Energetic Effects of Charge Reversal Mutations of Poxvirus Topoisomerase IB. *Biochemistry* **51,** 2940–2949 (2012).

59.   Perry, K., Hwang, Y., Bushman, F. D. & Van Duyne, G. D. Insights from the structure of a smallpox virus topoisomerase-DNA transition state mimic. *Structure* **18,** 127–137 (2010).

60.   Staker, B. L. *et al.* The mechanism of topoisomerase I poisoning by a camptothecin analog. *Proc Natl Acad Sci USA* **99,** 15387–15392 (2002).

61.   Basili, S. & Moro, S. Novel camptothecin derivatives as topoisomerase I inhibitors. *Expert Opin Ther Pat* **19,** 555–574 (2009).

62.   Stewart, L., Ireton, G. C., Parker, L. H., Madden, K. R. & Champoux, J. J. Biochemical and biophysical analyses of recombinant forms of human topoisomerase I. *J Biol Chem* **271,** 7593–7601 (1996).

63.   Koster, D. A., Palle, K., Bot, E. S. M., Bjornsti, M.-A. & Dekker, N. H. Antitumour drugs impede DNA uncoiling by topoisomerase I. *Nature* **448,** 213–217 (2007).

64.   Seol, Y., Zhang, H., Pommier, Y. & Neuman, K. C. A kinetic clutch governs religation by type IB topoisomerases and determines camptothecin sensitivity. *Proc Natl Acad Sci USA* **109,** 16125–16130 (2012).

65.   Leppard, J. B. & Champoux, J. J. Human DNA topoisomerase I: relaxation, roles, and damage control. *Chromosoma* **114,** 75–85 (2005).

66.   Stewart, L., Redinbo, M. R., Qiu, X., Hol, W. G. & Champoux, J. J. A model for the mechanism of human topoisomerase I. *Science* **279,** 1534–1541 (1998).

67.   Perry, K., Hwang, Y., Bushman, F. D. & Van Duyne, G. D. Structural basis for specificity in the poxvirus topoisomerase. *Mol Cell* **23,** 343–354 (2006).

68.   Muller, M. T. Quantitation of eukaryotic topoisomerase I reactivity with DNA. Preferential cleavage of supercoiled DNA. *Biochim Biophys Acta* **824,** 263–267 (1985).

69.   Camilloni, G., Di Martino, E., Di Mauro, E. & Caserta, M. Regulation of the function of eukaryotic DNA topoisomerase I: topological conditions for inactivity. *Proc Natl Acad Sci USA* **86,** 3080–3084 (1989).

70.   Nagarajan, R., Kwon, K., Nawrot, B., Stec, W. J. & Stivers, J. T. Catalytic phosphoryl interactions of topoisomerase IB. *Biochemistry* **44,** 11476–11485 (2005).

71.   Wereszczynski, J. & Andricioaei, I. Free energy calculations reveal rotating-ratchet mechanism for DNA supercoil relaxation by topoisomerase IB and its inhibition. *Biophys J* **99,** 869–878 (2010).

72.   Caserta, M., Amadei, A., Di Mauro, E. & Camilloni, G. In vitro preferential topoisomerization of bent DNA. *Nucleic Acids Res* **17,** 8463–8474 (1989).

73.   E L Zechiedrich, N. O. Eukaryotic topoisomerases recognize nucleic acid topology by preferentially interacting with DNA crossovers. *EMBO J* **9,** 4555 (1990).

74.   Krogh, S., Mortensen, U. H., Westergaard, O. & Bonven, B. J. Eukaryotic topoisomerase I-DNA interaction is stabilized by helix curvature. *Nucleic Acids Res* **19,** 1235–1241 (1991).

75.   Yang, Z. & Champoux, J. J. Assays for the preferential binding of human topoisomerase I to supercoiled DNA. *Methods Mol Biol* **582,** 49–57 (2009).

76.   K R Madden, L. S. J. J. C. Preferential binding of human topoisomerase I to superhelical DNA. *EMBO J* **14,** 5399 (1995).

77.   Yang, Z. *et al.* Recognition of forcible curvature in circular DNA by human topoisomerase I. *Chemical Communications* **47,** 11309–11311 (2011).

78.   Yang, Z., Li, D., Guo, J., Shao, F. & Li, T. Intrinsic curvature in duplex DNA inhibits Human Topoisomerase I. *Bioorg. Med. Chem. Lett.* **22,** 1322–1325 (2012).

79.   Yang, Z., Carey, J. F. & Champoux, J. J. Mutational analysis of the preferential binding of human topoisomerase I to supercoiled DNA. *FEBS J* **276,** 5906–5919 (2009).

80.   Litwin, T. R., Solà, M., Holt, I. J. & Neuman, K. C. A robust assay to measure DNA topology-dependent protein binding affinity. *Nucleic Acids Res* (2014).

81.   Moreno-Herrero, F. *et al.* Atomic force microscopy shows that vaccinia topoisomerase IB generates filaments on DNA in a cooperative fashion. *Nucleic Acids Res* **33,** 5945–5953 (2005).

82.   Shuman, S., Bear, D. G. & Sekiguchi, J. Intramolecular synapsis of duplex DNA by vaccinia topoisomerase. *EMBO J* **16,** 6584–6589 (1997).

83.   Subramani, R. *et al.* A novel secondary DNA binding site in human topoisomerase I unravelled by using a 2D DNA origami platform. *ACS Nano* **4,** 5969–5977 (2010).

84.   Patel, A., Yakovleva, L., Shuman, S. & Mondragón, A. Crystal structure of a bacterial topoisomerase IB in complex with DNA reveals a secondary DNA binding site. *Structure* **18,** 725–733 (2010).

85.   D'Annessa, I. *et al.* Simulations of DNA topoisomerase 1B bound to supercoiled DNA reveal changes in the flexibility pattern of the enzyme and a secondary protein-DNA binding site. *Nucleic Acids Res* **42,** 9304–9312 (2014).

86.   Shuman, S. Site-specific DNA cleavage by vaccinia virus DNA topoisomerase I. Role of nucleotide sequence and DNA secondary structure. *J Biol Chem* **266,** 1796–1803 (1991).

87.   Stivers, J. T., Shuman, S. & Mildvan, A. S. Vaccinia DNA topoisomerase I:

single-turnover and steady-state kinetic analysis of the DNA strand cleavage and ligation reactions. *Biochemistry* **33,** 327–339 (1994).

88. Woodfield, G., Cheng, C., Shuman, S. & Burgin, A. B. Vaccinia topoisomerase and Cre recombinase catalyze direct ligation of activated DNA substrates containing a 3'-para-nitrophenyl phosphate ester. *Nucleic Acids Res* **28,** 3323–3331 (2000).

89. Cheng, C. & Shuman, S. Recombinogenic flap ligation pathway for intrinsic repair of topoisomerase IB-induced double-strand breaks. *Mol Cell Biol* **20,** 8059–8068 (2000).

90. Stivers, J., Harris, T. & Mildvan, A. Vaccinia DNA Topoisomerase I: Evidence Supporting a Free Rotation Mechanism for DNA Supercoil Relaxation. *Biochemistry* (1997).

91. Shuman, S., Golder, M. & Moss, B. Characterization of vaccinia virus DNA topoisomerase I expressed in Escherichia coli. (1988).

92. Minkah, N. *et al.* Variola virus topoisomerase: DNA cleavage specificity and distribution of sites in Poxvirus genomes. *Virology* **365,** 60–69 (2007).

93. Shuman, S. Site-specific interaction of vaccinia virus topoisomerase I with duplex DNA. Minimal DNA substrate for strand cleavage in vitro. *J Biol Chem* **266,** 11372–11379 (1991).

94. Da Fonseca, F. & Moss, B. Poxvirus DNA topoisomerase knockout mutant exhibits decreased infectivity associated with reduced early transcription. *Proc Natl Acad Sci USA* **100,** 11291–11296 (2003).

95. Vandermeulen, G., Marie, C., Scherman, D. & Préat, V. New generation of

plasmid backbones devoid of antibiotic resistance marker for gene therapy trials. *Mol. Ther.* **19,** 1942–1949 (2011).

96. Mayrhofer, P., Schleef, M. & Jechlinger, W. in *Gene Therapy of Cancer* **542,** 87–104 (Humana Press, 2009).

97. Fogg, J. M. *et al.* Exploring writhe in supercoiled minicircle DNA. *J Phys Condens Matter* **18,** S145–S159 (2006).

98. Kay, M. A., He, C.-Y. & Chen, Z.-Y. A robust system for production of minicircle DNA vectors. *Nat Biotechnol* **28,** 1287–1289 (2010).

99. Zechiedrich, E. L., Khodursky, A. B. & Cozzarelli, N. R. Topoisomerase IV, not gyrase, decatenates products of site-specific recombination in Escherichia coli. *Genes Dev* **11,** 2580–2592 (1997).

100. Landy, A. Dynamic, structural, and regulatory aspects of lambda site-specific recombination. *Annual review of biochemistry* **58,** 913–949 (1989).

101. Bliska, J. B. & Cozzarelli, N. R. Use of site-specific recombination as a probe of DNA structure and metabolism in vivo. *J Mol Biol* **194,** 205–218 (1987).

102. Keller, W. Determination of the number of superhelical turns in simian virus 40 DNA by gel electrophoresis. *Proc Natl Acad Sci USA* **72,** 4876–4880 (1975).

103. Crawford, L. V. & Waring, M. J. Supercoiling of polyoma virus DNA measured by its interaction with ethidium bromide. *J Mol Biol* **25,** 23–30 (1967).

104. Fogg, J., Catanese, D., Randall, G. & Swick, M. Differences between positively and negatively supercoiled DNA that topoisomerases may distinguish. *Mathematics of DNA* (2009).

105. Kwon, K., Nagarajan, R. & Stivers, J. T. Ribonuclease activity of vaccinia DNA

topoisomerase IB: kinetic and high-throughput inhibition studies using a robust continuous fluorescence assay. *Biochemistry* **43,** 14994–15004 (2004).

106.   Vologodskii, A. V. & Cozzarelli, N. R. Conformational and thermodynamic properties of supercoiled DNA. *Annu Rev Biophys Biomol Struct* **23,** 609–643 (1994).

107.   Hernández, P. & Krimer, D. B. The benefit of DNA supercoiling during replication. *Biochemical Society* (2013).

108.   Schvartzman, J. B. & Stasiak, A. A topological view of the replicon. *EMBO Rep* **5,** 256–261 (2004).

109.   Veloso, A. *et al.* Genome-wide transcriptional effects of the anti-cancer agent camptothecin. *PLoS ONE* **8,** e78190 (2013).

110.   King, I. F. *et al.* Topoisomerases facilitate transcription of long genes linked to autism. *Nature* (2013).

111.   Ma, J., Bai, L. & Wang, M. D. Transcription Under Torsion. *Science* **340,** 1580–1583 (2013).

112.   Sternglanz, R. *et al.* Mutations in the gene coding for Escherichia coli DNA topoisomerase I affect transcription and transposition. *Proc Natl Acad Sci USA* **78,** 2747–2751 (1981).

113.   Wu, H. Y., Shyy, S. H., Wang, J. C. & Liu, L. F. Transcription generates positively and negatively supercoiled domains in the template. *Cell* **53,** 433–440 (1988).

114.   Norregaard, K. *et al.* DNA supercoiling enhances cooperativity and efficiency of an epigenetic switch. *Proc Natl Acad Sci USA* **110,** 17386–17391 (2013).

115. Vos, S. M., Tretter, E. M., Schmidt, B. H. & Berger, J. M. All tangled up: how cells direct, manage and exploit topoisomerase function. *Nat Rev Mol Cell Biol* **12,** 827–841 (2011).

116. Kwon, K. & Stivers, J. T. Fluorescence spectroscopy studies of vaccinia type IB DNA topoisomerase. Closing of the enzyme clamp is faster than DNA cleavage. *J Biol Chem* **277,** 345–352 (2002).

117. Shure, M. & Vinograd, J. The number of superhelical turns in native virion SV40 DNA and minicol DNA determined by the band counting method. *Cell* **8,** 215–226 (1976).

118. Gowetski, D. B., Kodis, E. J. & Kahn, J. D. Rationally designed coiled-coil DNA looping peptides control DNA topology. *Nucleic Acids Res* (2013).

119. Zhao, N., Fogg, J. M., Zechiedrich, L. & Zu, Y. Transfection of shRNA-encoding Minivector DNA of a few hundred base pairs to regulate gene expression in lymphoma cells. *Gene Ther* **18,** 220–224 (2011).

120. Vologodskii, A. V., Lukashin, A. V., Anshelevich, V. V. & Frank-Kamenetskii, M. D. Fluctuations in superhelical DNA. *Nucleic Acids Res* (1979).

121. Carey, J. F., Schultz, S. J., Sisson, L., Fazzio, T. G. & Champoux, J. J. DNA relaxation by human topoisomerase I occurs in the closed clamp conformation of the protein. *Proc Natl Acad Sci USA* **100,** 5640–5645 (2003).

122. Sherratt, M. J., Meadows, R. S., Graham, H. K., Kielty, C. M. & Holmes, D. F. ECM macromolecules: rotary shadowing and transmission electron microscopy. *Methods Mol Biol* **522,** 175–181 (2009).

123. Lesser, D. R., Kurpiewski, M. R. & Jen-Jacobson, L. The energetic basis of

specificity in the Eco RI endonuclease--DNA interaction. *Science* **250,** 776–786 (1990).

124. Lillian, T. D., Taranova, M., Wereszczynski, J., Andricioaei, I. & Perkins, N. C. A Multiscale Dynamic Model of DNA Supercoil Relaxation by Topoisomerase IB. *Biophys J* **100,** 2016–2023 (2011).

125. Baker, N. M., Rajan, R. & Mondragón, A. Structural studies of type I topoisomerases. *Nucleic Acids Res* **37,** 693–701 (2009).

126. Seol, Y. & Neuman, K. C. Single-molecule measurements of topoisomerase activity with magnetic tweezers. *Methods Mol Biol* **778,** 229–241 (2011).

127. Vologodskii, A. & Frank-Kamenetskii, M. D. Strong bending of the DNA double helix. *Nucleic Acids Res* **41,** 6785–6792 (2013).

128. Porecha, R. H. & Stivers, J. T. Uracil DNA glycosylase uses DNA hopping and short-range sliding to trap extrahelical uracils. *Proc Natl Acad Sci USA* **105,** 10791–10796 (2008).

129. Shlyakhtenko, L. S., Gall, A. A. & Lyubchenko, Y. L. in *Methods in Molecular Biology* **931,** 295–312 (Humana Press, 2012).

Curriculum Vitae

Breeana Grogan Anderson

527 F Street NE Apt #1   (949) 584-7171
Washington, DC 20002   breegrogan@gmail.com

SUMMARY

- Independent problem solver who answers scientific questions through creative method design
- Strong oral and written communicator of scientific concepts and data to technical and non-technical audiences
- Thorough data analyst capable of drawing meaningful conclusions from a variety of sources and models
- Researcher with experience interpreting a breadth of topics from biology, chemistry, and public health
- Demonstrated interest in the application of science to decision-making in policy and public health

EDUCATION

Johns Hopkins University, Baltimore, MD
Doctorate of Philosophy (PhD) in Chemical Biology   Expected April 2015
Master of Science in Chemical Biology   May 2011
Johns Hopkins Bloomberg School of Public Health, Baltimore, MD

Certificate in Risk Sciences and Public Policy   Expected May 2015
Georgetown University, Washington, DC   May 2009
Bachelor of Science in Biochemistry with a Certificate in Science, Technology, and International Affairs (Cum Laude)

PROFESSIONAL AND RESEARCH EXPERIENCE

Johns Hopkins University, Baltimore, MD
Graduate Student and NIH Predoctoral Fellow   August 2009-Present
<u>Research and Training</u> (Lab of James Stivers, Department of Pharmacology)

- Managed, performed, and completed multiple projects aimed at analyzing the regulation and mechanism of topoisomerase in interaction with supercoiled DNA, yielding one lead author publication
- Designed and optimized new protocols and adapted established methods for the purification of novel minicircle DNA substrates, improving the yield and speed of the experiment
- Collaborated as an integral part of a diverse team of graduate students to understand nucleotide pools in animal and human cell lines, resulting in one lead author paper
- Developed multiple ideas and concepts into a successful NIH training grant application totaling ~$125,000
- Conveyed research findings and methods orally and through posters sessions to engage scientists from varied backgrounds and levels of expertise

<u>Leadership, Teaching, Mentoring, and Community Engagement</u>

- Prepared experiments and advised undergraduate students on molecular biology as a teaching assistant
- Organized student-invited speaker seminars, planning two highly attended lectures given by top level scientists
- Mentored graduate students on numerous projects to improve their lab techniques and communication skills
- Maintained the lab budget and coordinated purchases among employees to manage costs and operations

- Actively engaged as a member of scientific societies such as AAAS by attending workshops to learn about science policy and advocate Congressional staff to recommend support for basic research
- Participant in the Johns Hopkins Science Policy and Advocacy Network, which is aimed at communicating biomedical research advances and benefits to a diverse audience from the general public and funding agencies

Smithsonian National Museum of Natural History, Washington, DC
Volunteer   December 2013 – Present
- Guided visitors through the scientific method in the "Q?rius" exhibit using interactive and hands-on learning tools
- Translated and adapted information from complex scientific disciplines into easy to understand language and visual aids to serve the non-technical general public
- Led discussions to improve understanding of the natural world and engage future generations of scientists

Georgetown University, Washington, DC
Undergraduate Researcher   January 2008-May 2009
Lab of Steve Metallo, Department of Biochemistry
- Performed and presented original research as a part of the NSF's Undergraduate Research Experience Program
- Wrote and defended an honors thesis on DNA-binding of intrinsically disordered proteins
- Served as Tutor Coordinator of the Chemistry Club, planning and leading weekly help sessions for fellow students

PEER-REVIEWED PUBLICATIONS

- **Anderson BG**, Stivers JT. "Variola Type IB DNA Topoisomerase: DNA Binding and Supercoil Unwinding Using Engineered DNA Minicircles." Biochemistry. 2014. 53(26):4302-15.
- **Grogan BC**, Parker JB, Guminski AF, Stivers JT. "Effect of the thymidylate synthase inhibitors on dUTP and TTP pool levels and the activities of DNA repair glycosylases on uracil and 5-fluorouracil in DNA." Biochemistry. 2011. 50(5):618-27.

FELLOWSHIPS AND AWARDS

- Finalist, Presidential Management Fellowship   April 2015
- NIH Ruth L. Kirschstein National Research Service Award for Predoctoral Fellowships to Promote Diversity in Health-Related Research (F31)   May 2012-May 2015
- Highlighted Article in *Biochemistry*   July 2014
- Participant, Student Workshop on Catalyzing Advocacy in Science and Engineering (AAAS)
                                                                                          April 2014
- American Institute of Chemists Student Award   May 2009
- Clare Booth Luce Scholarship for Women in Science, Mathematics, and Engineering
                                                                                August 2008-May 2009
- NIH Intramural Research Training Award   August 2007-December 2007

RELEVANT COURSEWORK

Public Health: Environmental Health, International Health, Epidemiology, Toxicology, Biostatistics, Risk Science and Public Policy, Risk Communication and Management, Risk Quantification
Chemical Biology: Methods in Molecular Biophysics, Inorganic Chemistry, Advanced Organic Chemistry, Bioinformatics, Chemical Biology, Proteins and Nucleic Acids, Genome Integrity and Cancer, Organic Mechanisms of Biology

TECHNICAL SKILLS

Certifications: Radiation Safety, Shipping of Hazardous Materials, and Responsible Conduct of Research
Laboratory Skills: Enzyme Kinetics, Molecular Cloning, Mutagenesis, DNA Isolation, Protein Expression and Purification, Protein and Nucleic Acid Gel Electrophoresis, UV/Vis and

Fluorescence Spectroscopy, High-throughput Screens, Autoradiography, Liquid Chromatography, and Human and Insect Cell Culture
Computer Skills: Microsoft Office Suite, Data Analysis and Curve-Fitting Software (Prism, PyMol, Quantity One, Image J), Data Modeling and Simulation Software (Dynafit, Crystal Ball), and Basic Programming (R)
Clearance: US Citizen with Level 1 Public Trust